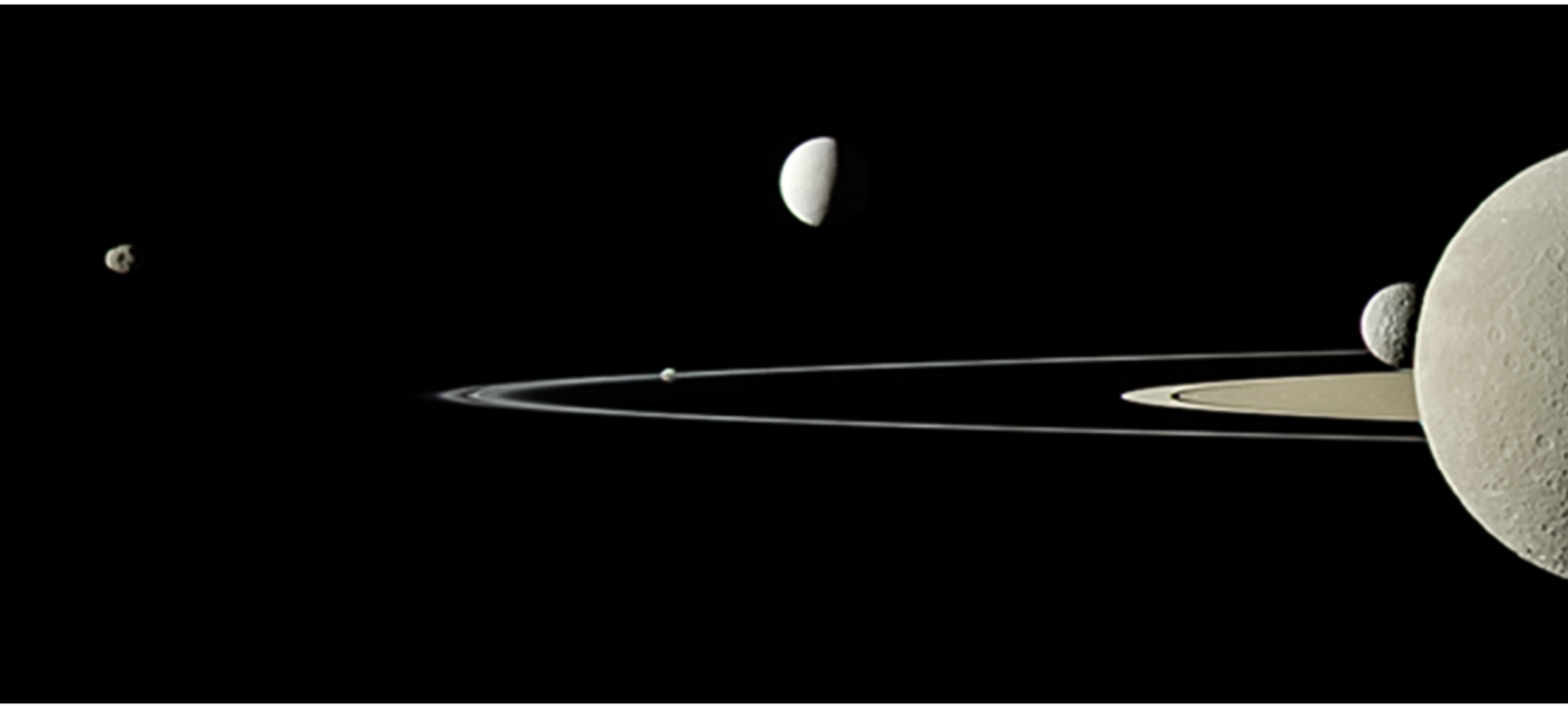

# ICY SATELLITES

The Voyager and Pioneer flybys of the 1970s and 1980s provided incomplete views of Saturn's moons. However, during its many years in Saturn orbit, Cassini discovered previously unknown moons, solved mysteries about known ones, studied their interactions with the rings and revealed how sharply different the moons are from one another. Saturn's moons range in size from about a third of a kilometer in size to larger than the planet Mercury, and they vary in color, texture and composition, and internal structure. Cassini data has also hinted at a possibly young age for several of the innermost icy moons.

For decades, scientists did not know why Enceladus was the brightest world in the solar system, or how it related to Saturn's E-ring. Cassini found that both the fresh coating on its surface, and icy material in the E-ring originate from vents connected to a global subsurface saltwater ocean that might host hydrothermal vents and complex organics.

The **Icy Satellites** Working Group (ISWG) working with the Satellites Orbiter Science Team (SOST) coordinated and implemented the icy satellite observation planning and detailed scheduling for the many icy satellite flybys throughout the mission, including 23 close Enceladus flybys, to ensure that Cassini icy satellite objectives were met. The ISWG Discipline Working Group (DWG) has achieved their Cassini mission objectives and has provided the first extended, comprehensive view of the moons of Saturn.

# CONTENTS



## Figures

## Tables

## Executive Summary

The Cassini-Huygens mission offered the first extended, comprehensive view of the moons of Saturn. There are existing and upcoming review books and papers that summarize the results from the Cassini mission; as is the case with so many previous missions, major questions remain even after more than a dozen years of exploration [Buratti et al. 2017]. The questions appropriate to the icy satellite discipline that were proposed at the onset of the mission were far-reaching science goals that provided the driving force behind the mission are listed in the section entitled Key Objectives for Icy Satellites DWG, and summarized in Spilker [1997]. As the section entitled Icy Satellites Science Assessment shows, most mission objectives were fully met with only two (not including two objectives associated with asteroid science) partially met. The asteroid flyby investigations were lacking because the spacecraft trajectory did not bring Cassini sufficiently close to an object in the Main Belt.

> … far-reaching science goals provided the driving force behind the mission …

## Key Objectives for Icy Satellites DWG

### Icy Satellites AO Objectives

- **Icy Satellite Geology and History (I_AO1)** – Determine the general characteristics and geological histories of the satellites.
- **Icy Satellite Surface and Crustal Modifications (I_AO2)** – Define the mechanisms of crustal and surface modifications, both external and internal.
- **Icy Satellite Surface Composition (I_AO3)** – Investigate the compositions and distributions of surface materials, particularly dark, organic rich materials and low melting point condensed volatiles.
- **Icy Satellite Interior Properties (I_AO4)** – Constrain models of the satellites' bulk compositions and internal structures.
- **Icy Satellite Magnetosphere and Ring Interactions (I_AO5)** – Investigate interactions with the magnetosphere and ring systems and possible gas injections into the magnetosphere.

### Icy Satellites CSM Traceability Matrix Objectives

- **Enceladus Seasonal Changes (IC1a)** – Identify long-term secular and seasonal changes at Enceladus through observations of the south polar region, jets, and plumes, and through analysis of heat production.

- **Enceladus Ocean (IN1a)** – Determine the presence of an ocean at Enceladus as inferred from induced magnetic field and plume composition, search for possible anomalies in the internal structure of Enceladus as associated with plume sources, and constrain the mechanisms driving the endogenic activity by in situ observations and remote sensing.
- **Mid-sized Satellites (IN1b)** – Complete the comparative study of Saturn's mid-sized satellites, their geological and cratering histories, and interactions with the Saturn system, with remote sensing of Mimas at the highest resolution possible in order to understand the mechanisms behind its unique thermal properties discovered by Cassini. Understand if other moons exhibit similar thermal properties.
- **Dione (IN1c)** – Determine whether Dione exhibits evidence for low-level activity, now or in recent geological time.
- **Rhea (IN2a)** – Determine whether there is ring material orbiting Rhea, and if so, what its spatial and particle size distribution is. Understand the origin of blue pearls discovered on its surface.
- **Tethys (IN2b)** – Determine whether Tethys contributes to the E-ring and the magnetospheric ion and neutral population. Understand the nature of mysterious red streaks discovered on its surface.
- **Satellite Interiors (IN2c)** – Determine the extent of differentiation and internal inhomogeneity within the icy satellites, especially Rhea and Dione. Determine whether Dione has a subsurface ocean.
- **Small Moons (IN2d)** – Observe selected small satellites to quantify the movement of Enceladus material through the system, the history of satellite collisions/breakup, interaction with ring material as indicated by surface properties/composition, and cratering rates deep in the Saturnian system. Understand the composition of these moons and how it relates to kindred bodies in the Saturnian system and beyond.
- **Hyperion (IN2e)** – Understand the unusual appearance of Hyperion with remote sensing observations of the highest resolution possible.
- **Iapetus (IN2f)** – Use remote sensing of Iapetus to test models for the albedo heterogeneity of the satellite. Quantify the effect of the newly-discovered Phoebe ring on the properties of Iapetus' surface.

## Jupiter Flyby AO Objectives

- **Jupiter and Satellite Studies (J_AO1)** – Extend the time for studies of atmospheric dynamics and variable satellite phenomena, specifically Io volcanism, beyond the period accessible to the Galileo nominal mission.

## Asteroid Flyby AO Objectives

- **Asteroid Flyby Investigation (A_AO1)** – Investigate an asteroid not seen by previous missions, possibly a new class of asteroid, thereby adding important new information to the study of asteroid
- **Asteroid Global Characteristics (A_AO2)** – Characterize global properties, determine composition and morphology of the surface, investigate properties of the regolith.

## Icy Satellites Science Assessment

All these objectives have been answered to a large degree (see Table IcySats-1), and specific results can be expressed by this top twenty list of discoveries:

- Discovery of Enceladus jets, their coincidence with small-scale hot spots, the plume they form, and its impact on the Saturnian system.
- Evidence of hydrothermal chemistry and discovery of a strong thermal anomaly on Enceladus.
- Detection of global oceans beneath Enceladus's, and possibly Dione's and Mimas's icy crusts.
- Plume structure connection to both individual jets and curtains along tiger stripes.
- Plume strength modulation by tidal forces and stochastic on/off timing of individual jets.
- The plume of Enceladus as the source of the E-ring of Saturn.
- Detection of plume composition: water (vapor and micron-sized grains), salt, organics, nanograin dust, hydrogen, and ammonia.
- Discovery of supersonic motion in the jets.
- Evidence for subdued ongoing or recently extinguished activity on Dione.
- Red streaks on Tethys signifying potential outgassing along fractures.
- Accretion disks on the ring moons showing they continue to add particles from the main ring system to their bodies.
- Low densities of the small moons.
- Discovery of a globe-girdling equatorial ridge on Iapetus, perhaps akin to those seen on the ring moons.
- Thermal segregation and Phoebe ring particle infall as the cause of the bright/dark dichotomy on Iapetus, first discovered by the astronomer Cassini in 1677.
- Likely formation of Phoebe in the Kuiper Belt.

- The discovery that the high reflectance and albedo/color patterns of the Saturnian inner moons is primarily due to exchange of material between rings and moons specific to the Saturnian system. This includes the accumulation of E-ring particles and subsequent alteration by high-energy elections to produce Pac-Man.
- Discovery of organics and carbon dioxide (and possibly ammonia) on the outer moons. Evidence for iron oxides and space-weathered silicates on the surfaces of Phoebe and Iapetus.
- Wispy streaks on Dione and Rhea are actually fracture systems.
- Evidence for past rings around moons, such as blue pearls on Rhea, and possibly the ridge of Iapetus.
- Evidence that outer irregular moons are low density and slow rotators based on light curve surveys.

It was known before the Cassini mission that the main constituent of the surfaces of the moons is crystalline water ice. $CO_2$ is present on the surface of most of the moons [Buratti et al. 2005; Brown et al. 2006; Clark et al. 2012, 2008, 2005; Cruikshank et al. 2010], but there are still spectral identifications that are uncertain. Clark et al. [2012] showed that a weak feature at 2.42 μm is due to trapped molecular hydrogen and is observed in dark material on multiple icy satellites, but this feature needs confirmation by an independent instrument. A weak absorption at 2.97 μm corresponds to ammonia [Clark et al. 2012, 2008] and is seen on multiple icy satellites, but the absorption overlaps an order-sorting filter gap in the VIMS instrument where instrument errors are larger. Observations of ammonia need confirmation either by a better calibration of the VIMS data, or by other instruments.

An up-to-date table of the physical and dynamical properties of all the Saturnian moons is given at https://ssd.jpl.nasa.gov/?sat_elem and at https://ssd.jpl.nasa.gov/?phys_data.

The results of the mission can be summarized by Table IcySats-1. The colors refer to the data gathered and the expected results to be obtained by ongoing analyses. Green means the objective was fully met; yellow means it was partially met by the best estimate; and red means it was not met. Note that this assessment is based on whether sufficient data was collected, not on the status of the ongoing analysis and modeling of the data. The first five goals were set out in the mission Announcement of Opportunity, while subsequent goals in the table followed up in Cassini's extended mission on major discoveries. Text below primarily addresses the achievement of the extended mission goals.

**Table IcySats-1. Assessment of Mission Goals.**

**Fully/Mostly Accomplished:** **Partially Accomplished:** **Not Accomplished:**

| Icy Satellite Science Objectives | AO and TM Science Objectives | Icy Satellite Science Assessment | Comments |
|---|---|---|---|
| Icy Satellite Geology and History: (I_AO1) – Determine the general characteristics and geological histories of the satellites. | I_AO1 | | |

**Table IcySats-1. Assessment of Mission Goals.**

**Fully/Mostly Accomplished:** **Partially Accomplished:** **Not Accomplished:**

| Icy Satellite Science Objectives | AO and TM Science Objectives | Icy Satellite Science Assessment | Comments |
|---|---|---|---|
| Icy Satellite Surface and Crustal Modifications (I_AO2) – Define the mechanisms of crustal and surface modifications, both external and internal. | I_AO2 | | |
| Icy Satellite Surface Composition (I_AO3) – Investigate the compositions and distributions of surface materials, particularly dark, organic rich materials and low melting point condensed volatiles. | I_AO3 | | |
| Icy Satellite Interior Properties (I_AO4) – Constrain models of the satellites' bulk compositions and internal structures. | I_AO4 | | |
| Icy Satellite Magnetosphere and Ring Interactions (I_AO5) – Investigate interactions with the magnetosphere and ring systems and possible gas injections into the magnetosphere. | I_AO5 | | |
| Enceladus Seasonal Changes (IC1a) – Identify long-term secular and seasonal changes at Enceladus through observations of the south polar region, jets, and plumes. | IC1a | | |
| Enceladus Ocean (IN1a) – Determine the presence of an ocean at Enceladus as inferred from induced magnetic field and plume composition, search for possible anomalies in the internal structure of Enceladus as associated with plume sources, and constrain the mechanisms driving the endogenic activity by in situ observations and remote sensing. | IN1a | | |
| Mid-sized Satellites (IN1b) – Complete the comparative study of Saturn's mid-sized satellites, their geological and cratering histories, and interactions with the Saturn system, with remote sensing of Mimas at the highest resolution possible in order to understand the mechanisms behind its unique thermal properties discovered by Cassini. | IN1b | | |
| Dione (IN1c) – Determine whether Dione exhibits evidence for low-level activity, now or in recent geological time. | IN1c | | Extensive data were gathered, but the results are still ambiguous. No current activity was detected. |
| Rhea (IN2a) – Determine whether there is ring material orbiting Rhea, and if so, what its spatial and particle size distribution is. | IN2a | | |

**Table IcySats-1. Assessment of Mission Goals.**

**Fully/Mostly Accomplished:** **Partially Accomplished:** **Not Accomplished:**

| Icy Satellite Science Objectives | AO and TM Science Objectives | Icy Satellite Science Assessment | Comments |
|---|---|---|---|
| Tethys (IN2b) – Determine whether Tethys contributes to the E-ring and the magnetospheric ion and neutral population. | IN2b | | From a CDA/icy dust perspective, it is red because during the solstice mission there were no close Tethys flybys to measure potential ejecta [Kempf et al. 2010]. For MAPS as a whole, enough data was obtained to determine that Tethys does not contribute to the E-ring and magnetospheric ion and neutral population [Burch et al. 2007; Khurana et al. 2008]. |
| Satellite Interiors (IN2c) – Determine the extent of differentiation and internal inhomogeneity within the icy satellites, especially Rhea and Dione. | IN2c | | |
| Small Moons (IN2d) – Observe selected small satellites to quantify the movement of Enceladus material through the system, the history of satellite collisions/breakup, interaction with ring material as indicated by surface properties/composition, and cratering rates deep in the Saturnian system. | IN2d | | |
| Hyperion (IN2e) – Understand the unusual appearance of Hyperion with remote sensing observations of the highest resolution possible. | IN2e | | |
| Iapetus (IN2f) – Use remote sensing of Iapetus to test models for the albedo heterogeneity of the satellite. Quantify the effect of the newly-discovered Phoebe ring on the properties of Iapetus' surface. | IN2f | | |
| Jupiter and Satellite Studies (J_AO1) – Extend the time for studies of atmospheric dynamics and variable satellite phenomena, specifically Io volcanism, beyond the period accessible to the Galileo nominal mission. | J_AO1 | | |
| Asteroid Flyby Investigation (A_AO1) – Investigate an asteroid not seen by previous missions, possibly a new class of asteroid, thereby adding important new information to the study of asteroid | A_AO1 | | This objective was present for the case where Cassini would have flown close to an asteroid. No asteroid was found to be nearby. |
| Asteroid Global Characteristics (A_AO2) – Characterize global properties, determine composition and morphology of the surface, investigate properties of the regolith. | A_AO2 | | This objective was present for the case where Cassini would have flown close to an asteroid. No asteroid was found to be nearby. |

# ICY SATELLITES DWG SYSTEM RESULTS

## Enceladus Seasonal Changes (IC1a)

Enceladus eruptions are mostly water vapor, with a variable amounts of micron-sized ice grains [Porco et al. 2017, 2006; Hedman et al. 2018]. There are ~100 discrete jets and faint sheets of icy particles fountaining from the four tiger stripe fissures across Enceladus' south polar region [Porco et al. 2014; Spitale et al. 2015; Teolis et al. 2017].

The brightness, and hence mass, of the plume created by the particle jets varies diurnally, most likely due to the cycling of tidal extensional/compressional stresses across the south polar terrain [Hedman et al. 2013; Nimmo et al. 2014]. A phase lag of ~45 deg (or ~4.5 hours), compared to the ice-shell response predicted by simple tidal models for an elastic ice shell, is present though its origin is not clear [Nimmo et al. 2014]. Notable is the observation that the plume never goes to zero strength, as seen in particles [Nimmo et al. 2014] as well as vapor [Hansen et al. 2017]. Individual geysers were observed to be time variable, turning on and/or off on timescales that were not comparable to the diurnal cycling of stresses [Porco et al. 2014; Teolis et al. 2017]. This was taken as an indication that condensation of ice in the vents leads to the stochastic clogging of the vents and consequently the shutoff of geysers, but averaged across the SPT, the plume is continuous in time if variable in strength. The estimated timescale for the clogging process is months to a couple of years [Porco et al. 2014, 2006].

Behounkova et al. [2015], in a 3-D numerical model of the viscoelastic tidal response of the ice shell, showed the diurnal brightness variation is best described by the cycling of the normal stresses across the fractures averaged over the SPT. They proposed that the delay in eruption activity may be a natural consequence of the viscosity structure in the south polar region and the size of the putative subsurface ocean, but there are alternate suggestions [Kite and Rubin 2016].

One hot spot was identified on Enceladus with radar observations [Le Gall et al. 2017]. VIMS data were able to place constraints on the size and temperature of one opening, just 9 m wide [Goguen et al. 2013]. VIMS observations of hot spots [Goguen et al. 2013] were used in conjunction with Imaging Science Subsystem (ISS) observations to show that individual jets are spatially coincident with the small-scale (~10 s meters) hot spots [Porco et al. 2014], a result that indicates the heat emerging from the fractures is largely that due to the latent heat of condensation of vapor in the near-surface portion of the vents, and not due to shear heating, and is consistent with a deep source of the eruptive materials.

An analysis of ISS observations of the plume from 2005–2015 suggested there may be seasonal changes in the plumes' brightness.

An analysis of ISS observations of the plume from 2005–2015 suggested there may be seasonal changes in the plumes' brightness [Ingersoll and Ewald 2017] (Figure ICYSATS-1). However, a later analysis of the full suite of Cassini ISS plume observations through the end of the

mission (August 2017) has shown that the long-timescale variations in the plume's brightness are most likely due to two periods (4-year and 11-year) both associated with the Dione-Enceladus 2:1 orbital resonance that also cause the cycling of tidal stresses across the moon's surface [Porco et al. 2018].

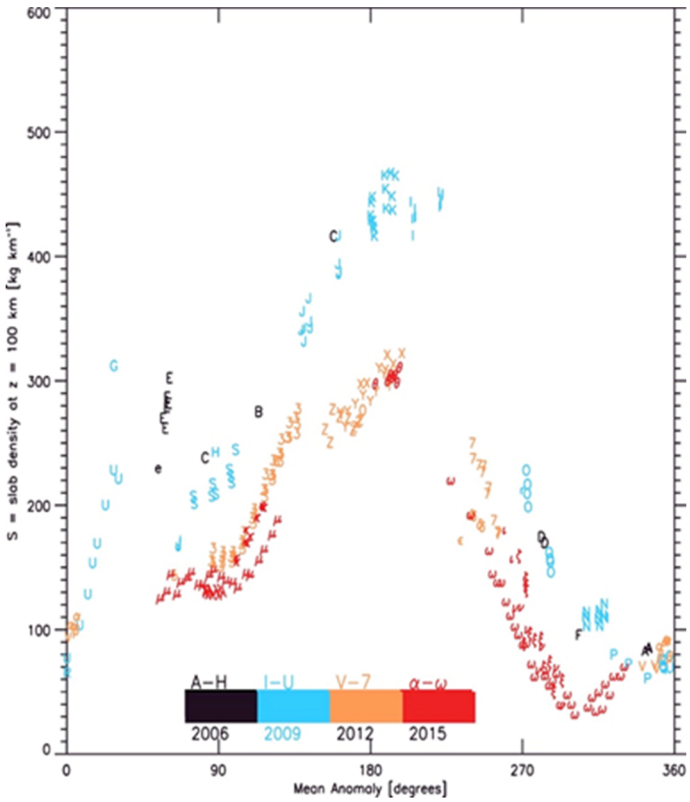


**Figure ICYSATS-1. A figure of plume brightness from 2006 through 2015 showing year-to-year changes in the amplitude of the diurnal variations with mean anomaly, including a substantial decrease toward the end of the mission. Figure from Ingersoll and Ewald [2017].**

Composite Infrared Spectrometer (CIRS) also carried out a significant investigation on the variability of heat in the tiger stripe region throughout the mission on various time scales, with special focus on this problem at the end of the mission [Howett et al. 2017]. CIRS observations of Enceladus' active south polar region during Cassini's F-ring and Proximal Orbits (FRPO) were designed to investigate whether Enceladus' surface temperatures also vary with time. Preliminary results indicate that Enceladus' surface temperatures vary with mean anomaly, but lag in time behind the plume brightness change. The total heat flux varied by about a factor of two with mean anomaly. A detailed measurement of the heat flux between revs 61 and 91 showed no significant change. Work is continuing in this area, as different analysis techniques give substantially different results for the heat flux (details are in the CIRS Science Results).

A series of Ultraviolet Imaging Spectrograph (UVIS) stellar and solar occulations were spectacularly successful for studying the composition and structure of Enceladus' plume [Hansen et al. 2011, 2008, 2006]. Unlike ISS and CIRS, UVIS detected no significant variations in the

amount of water vapor as seen over the course of the mission, although the strongest jets, which lift the most icy grains, are more variable [Hansen et al. 2017].

## Enceladus Ocean (IN1a)

Though the presence of liquid water within the conduits leading to the south polar surface, and then later the proposal that there was liquid water under the ice shell, were suggested early in the mission [Porco et al. 2006; Collins and Goodman 2007; Postberg et al. 2009], the first detection of this long-suspected body of liquid water beneath the moon's crust came from radio science data that showed Enceladus' gravity field combined with topography was consistent with a regional sea beneath Enceladus' south pole, though a global ocean could not be ruled out [Iess et al. 2014]. Subsequent, careful analysis of the rotational motion of Enceladus revealed a libration indicating the ice shell is decoupled from the core and the subsurface liquid ocean is global, as shown in Figure ICYSATS-2 [Thomas et al. 2015]. Figure ICYSATS-2 is a Cassini nugget summarizing our knowledge of the Enceladan Ocean.

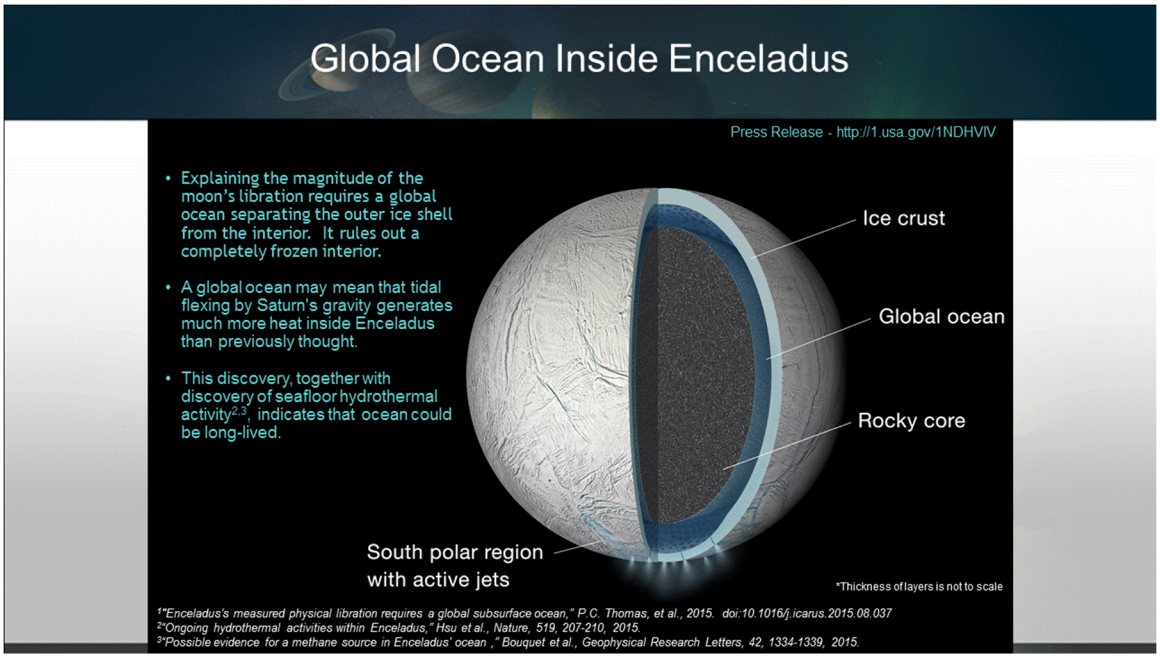


**Figure ICYSATS-2. A NASA Nugget summarizing our knowledge of the ocean of Enceladus at the end of the mission.**

Cassini's dust analyzer (CDA) determined the particle size and compositional profile for the water ice particles expelled from the tiger stripe fissures [Postberg et al. 2011]. Grain sizes are stratified: the smallest pure-ice particles (< 0.4 micron) condense from gas in the plume, reach escape velocity and go into orbit around Saturn, forming the E-ring. These tiny particles are likely lofted by the supersonic gas jets detected by UVIS [Hansen et al. 2011]. Larger salt-rich particles come from liquid water and may originate as a frozen aerosol spray, which is then carried by the

escaping gas to the surface. These larger grains separate from the gas, fall back to the surface and modify Enceladus' color [Schenk 2014; Postberg et al. 2017].

Observational constraints are necessary to develop models of the nature of the plumbing from the subsurface body of water to the nozzles carrying gas and particles to the surface [Teolis et al. 2017]. Several concepts for the nature of the plumbing that connects the subsurface liquid reservoir to the escaping gas and particles have been proposed. An early idea was a Perrier ocean powered by escaping $CO_2$: as seawater nears the surface pressure decreases, the dissolved gases come out of solution and bubbles form [Matson et al. 2012]. Another hypothesis is that the gas is accelerated as it goes through nozzle-like channels from the ocean to the surface [Schmidt et al. 2009; Yeoh 2017]. Yet another idea is that water coming up from the ocean separates the solid edges of the fissures and that tidal stresses partially open and close the fissures, keeping the water from freezing [Kite and Rubin 2016].

CDA detected silica nano-particles, confirming that the liquid layer is in contact with the rocky core.

CDA detected silica nano-particles, confirming that the liquid layer is in contact with the rocky core [Hsu et al. 2015]. Very hot water (194° F) is required for these particles to form, suggesting that Enceladus has hydrothermal vents on its seafloor. Furthermore, the abundance of methane gas in the plume can only happen if there are hydrothermal vents preventing the methane from being captured in the icy walls confining the ocean [Bouquet et al. 2015].

What is the pH of Enceladus' ocean? Values reported range from 8 [Hsu et al. 2015] to 12 [Glein et al. 2015], however the most likely range is 9–11 [Waite et al. 2017].

Another important result is provided by the Ion and Neutral Mass Spectrometer (INMS) detection of $H_2$. The process that likely provides the $H_2$, serpentinization of rock, could provide the chemical energy required for life [Waite et al. 2017]. Cassini's investigations have shown that Enceladus' ocean is a habitable environment.

## Mid-sized Satellites (IN1b)

The mid-sized bodies of Saturn proved to be a collection of unique bodies, ranging from Phoebe, a heavily cratered, relatively dense moon that is probably a captured Kuiper Belt object (KBO) [Johnson and Lunine 2005a] to less dense moons that may have some type of ongoing activity. The optical properties of the surfaces of these moons are largely determined by interactions with rings and high-energy particles. Accurate values for fundamental whole-body physical properties of the moons were obtained. These include mean radii, densities, and shapes—for example, Thomas [2010]; Thomas et al. [2018]; Castillo-Rogez et al. [2018]—and also photometric quantities such as geometric albedo, the phase integral, or Hapke photometric model parameters [Pitman et al. 2013; Verbiscer et al. 2018].

The sizes and shapes of the six mid-sized icy satellites were measured from ISS data. Mimas, Enceladus, Tethys, Dione, and Rhea are well described by triaxial ellipsoids; Iapetus is best represented by an oblate spheroid [Thomas et al. 2007]. Impact craters dominate the surfaces and provide the primary means of estimating terrain ages as well as many other properties of the surfaces [Dones et al. 2009; Kirchoff and Schenk 2010; Schenk et al. 2018; Kirchoff et al. 2018].

None of the unusual crater landforms (such as multi-ring basins or shallow distorted craters on the Galilean moons) seen on icy worlds that have confirmed internal oceans are seen on the mid-sized moons. However, this finding does not preclude possible oceans [Schenk et al. 2018]. Global mapping has revealed geologically complex worlds. All (except perhaps Iapetus) have been tectonically deformed to different degrees. Almost all tectonic landforms are interpreted as extensional structures [Schenk et al. 2018].

All of the icy Saturnian moons are absorbing in the ~0.2–0.5 μm region, making them dark at FUV wavelengths.

The trailing sides of Tethys and Dione, and to a lesser degree of Rhea, are darker than the respective leading sides. This is due to E-ring material infalling preferentially on the leading sides and has originally been discovered in Voyager data [Buratti et al. 1990]. The colors of the trailing sides are also redder than the leading sides of these moons.

All of the icy Saturnian moons are absorbing in the ~0.2–0.5 μm region, making them dark at far ultraviolet (FUV) wavelengths. For instance, Filacchione et al. [2016, 2012] used Cassini VIMS data to show that the spectral slope (0.35–0.55 μm) increases (becomes redder) with distance from Enceladus. While the ultraviolet (UV) absorber causes reddening, sub-micron grains induce increased scattering, causing a bluing effect, so there are competing signatures of these two components throughout the Saturn system.

Deuterium has been found on Phoebe, Iapetus, Hyperion, Rhea, Dione, Enceladus, and the Rings, and carbon 13 has been detected on Phoebe and Iapetus [Clark et al. 2019, 2017a, 2017b, 2016a, 2016b], and the deuterium to hydrogen (D/H) ratio derived. Phoebe is an outlier with D/H more than eight times higher than terrestrial, which the other satellites and rings are close to terrestrial ocean water values, an unexpected result not predicted by current models of solar system formation.

Infrared (IR) spectroscopy is sensitive to grain size of materials, and the multiple absorption in ice allows grain size mapping to be done with VIMS data. On Enceladus, the sizes of ice particles are generally well correlated with geologic features and surface ages, indicating a stratigraphic correlation between tectonic features and cryovolcanic activities [Jaumann et al. 2008]. Grains much smaller than the wavelength of light cause enhanced blue scattering, including a Rayleigh scattering effect. This bluing effect is observed in the Saturn system and quantified by Clark et al. [2012, 2008].

Scipioni et al. [2017] produced image cube maps of Enceladus, and mapped ice grain sizes and identified plume deposits across the surface. The map of the band-depth ratio 1.50/2.02 μm overall shows good agreement with the predicted plumes' deposits on the trailing side, where the amount of sub-micron particles decreases with increasing accumulation of ejecta material. However, this correlation is much weaker, or even absent, on the leading side of Enceladus, where the abundance of sub-micron particles is the highest across the entire surface.

Stephan et al. [2012] showed that the distribution of spectral endmembers as well as global band depth variations of Dione's water ice absorptions measurements imply that the bombardment with charged particles from Saturn's magnetosphere is one of at least two major global processes affecting Dione's surface. Ice deposits dominating its leading hemisphere appear rather associated with rays of the fresh impact crater Creusa on the northern leading hemisphere. These rays cross almost the whole hemisphere masking here any effects of possibly existent but less dominant processes as evident in the transition from the bright to dark regions on the Saturn-facing hemisphere (~0° W). $CO_2$ is evident in the dark material pointing to a possible formation due to the interaction of the surface material with the impacting particles from Saturn's magnetosphere. Local spectral differences are consistent with impacting particles from the trailing side as described by Clark et al. [2008] with a pronounced ice signature on crater walls facing the leading side direction and shielded from impacting particles and dark material concentrated on interior crater walls facing the trailing hemisphere.

Spectra of ice also varies with temperature, so the surface temperatures of cold icy surfaces can be sensed without needing to measure longer wavelength thermal emission. Filacchione et al. [2016] analyzed the ice spectral to produce daytime temperature maps of the satellite surfaces. Just one more indication of the diversity of science that an imaging spectrometer can provide.

Cassini radar tracks on Saturn's icy satellites through the end of the Prime Mission increased the number of radar albedo estimates to 73.

Cassini radar tracks on Saturn's icy satellites through the end of the Prime Mission increased the number of radar albedo estimates to 73 [Ostro et al. 2010]. The measurements sample diverse subradar locations (and for Dione, Rhea, and Iapetus, almost always use beamwidths less than half the target angular diameters), thereby constraining the satellites' global radar albedo distributions. The echoes result predominantly from volume scattering, and their strength is thus strongly sensitive to ice purity and regolith maturity. The combination of the Cassini data set and Arecibo 13-cm observations of Enceladus, Tethys, Dione, Rhea [Black et al. 2007], and Iapetus [Black et al. 2004] discloses an unexpectedly complex pattern of 13 cm to 2 cm wavelength dependence. The 13-cm albedos are generally smaller than 2-cm albedos and lack the correlation seen between 2 cm and optical geometric albedos. Enceladus and Iapetus are the most interesting cases. The E-ring has a prominent effect on the 13-cm radar lightcurve. The uppermost trailing-side regolith is too fresh for meteoroid bombardment to have developed larger-scale heterogeneities that would be necessary to elevate the 13-cm radar albedo, whereas all of Enceladus is clean and mature enough for the 2-cm albedo to be uniformly high. For, Iapetus, the

2-cm albedo is strongly correlated with optical albedo: low for the optically dark, leading-side material and high for the optically bright, trailing-side material. However, Iapetus' 13-cm albedo values show no significant albedo dichotomy and are several times lower than 2-cm values, being indistinguishable from the weighted mean of 13-cm albedos for main-belt asteroids, 0.15 ±0.10.

A series of UVIS stellar and solar occulations were designed at a wide range of latitudes and longitudes to search for thin atmospheres and plumes indicating possible activity.

The leading side's optically dark contaminant must be present to depths of at least one to several decimeters. A more detailed review of Cassini Radar observations of the icy moons of Saturn is detailed in the RADAR Instrument Science Results.

A series of UVIS stellar and solar occulations were designed at a wide range of latitudes and longitudes to search for thin atmospheres and plumes indicating possible activity. (The Planetary Data System (PDS) includes a list of these occultations.) This technique was spectacularly successful for Enceladus [Hansen et al. 2006]. Searches at Tethys, Iapetus, Rhea, and Dione showed no detectable atmosphere [Hansen et al. 2018].

Under the leadership of the inimitable Amanda Hendrix, UVIS set a gallant lead in obtaining full longitudinal and phase angle coverage of the icy satellites during the long mission, with CIRS, VIMS, and ISS benefitting from ride-a-long observations. The strong UV water absorption band is diagnostic of water ice, a major component of all the icy surfaces. This allows significant constraints on the surface composition and the processes that control the evolution of their surfaces [Hendrix and Hansen 2010, 2008; Hendrix et al. 2018, 2017, 2012; Royer and Hendrix 2014].

Substantial effort was expended on understanding the thermal properties of the medium-sized moons. Observations returned by CIRS and ISS showed a thermal and color anomaly at low latitudes on Mimas and Tethys' leading hemisphere, dubbed Pac-Man, because its shape mimics that of the 1980s' video icon (Figure ICYSATS-3). Pac-Man display warmer nighttime and cooler daytime temperatures than its surroundings and appears darker in IR/UV color ratio maps [Howett et al. 2012, 2011; Schenk et al. 2011]. The color and thermal anomalies are believed to be the result of surface alteration by high-energy electrons, which preferentially bombard this region, altering its surface and increasing its thermal inertia. These high-energy electrons, in Saturn's magnetosphere, drift in a retrograde direction relative to corotation. Recent modeling efforts, supported by the Low Energy Magnetospheric Measurement System (LEMMS) on Cassini's Magnetospheric Imaging Instrument (MIMI), have shown that these electrons preferentially bombard low latitudes on Mimas, Tethys, and Dione's leading hemisphere [Paranicas et al. 2014, 2012; Howett et al. 2011; Schenk et al. 2011]. The thermal anomaly is closely correlated spatially with an IR/UV (0.930/0.338 lm) color ratio anomaly previously observed in global maps of Mimas using Cassini ISS data.

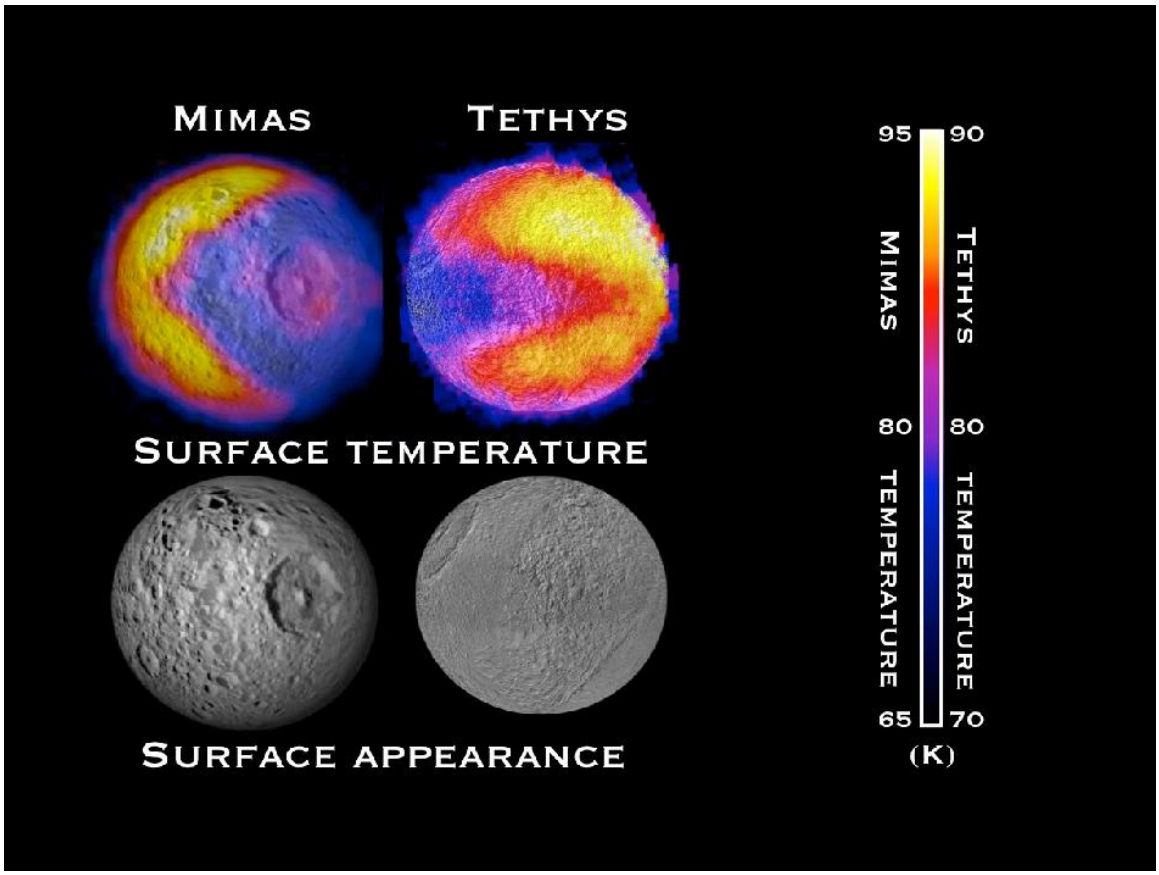


**Figure ICYSATS-3. Pac-Man on Mimas and Tethys.**

CIRS also measured the bolometric Bond albedo, the thermal inertia, and skindepths of the moons, which are summarized in Table ICYSATS-2 [Howett et al. 2010]. The thermal inertia of all of Saturn's icy satellites is shown to be less than half that of the Galilean satellites, implying less consolidated and more porous surfaces, perhaps partially due to the limited mobility of water ice on the Saturnian satellites due to their low temperatures compared with the Galilean satellites, or to a surface coating of E-ring particles. The latitudinal variation in the thermal inertia of Enceladus implies the surface becomes more consolidated towards the southern pole, whereas the higher albedo in the southern hemisphere implies a cleaner surface, perhaps due to plume fallout. Further work investigating the hemispheric bolometric Bond albedo asymmetries of Dione would be valuable, as although the globally averaged values derived here provide a good fit to the CIRS data, observations of viable wavelength have observed notable differences between the leading and trailing hemispheres [Buratti and Veverka 1984].

In September 2011 (during Cassini's orbit 153), CIRS obtained a daytime medium-spatial resolution observation (the average resolution was 84 km/pixel) of Tethys' leading hemisphere [Howett et al. 2012]. The results clearly show that a thermally anomalous Pac-Man region exists on Tethys' leading hemisphere at low latitudes in both the daytime and nighttime temperatures. The region appears to be ~10 K cooler during the day and ~10 K warmer at night than its

surroundings, quite unlike the pattern expected if surface properties were spatially uniform. The largest thermal contrast occurs at the northern anomaly boundary, particularly towards the east. The thermally anomalous region is lens-shaped with apexes at 0° W and 180° W, and is widest in the center of the leading hemisphere (90° W) reaching latitude ±20°. This anomalous region spatially coincides with a dark (low) albedo region at low latitudes on Tethys' leading hemisphere was first observed in Voyager data [Buratti and Veverka 1984; Buratti et al. 1990; Stooke 2002, 1989]. Photometry applied to Cassini ISS images showed the band to be 2–3% brighter in the narrow angle camera (NAC) CL1-UV3 filter (338 nm) and 8% darker in the NAC CL1-IR3 (930 nm) filter [Elder et al. 2007].

A Pac-Man thermal anomaly was also detected on Mimas [Howett et al. 2011]. It is closely correlated spatially with an IR/UV (0.930/0.338 lm) color ratio anomaly previously observed in global maps of Mimas using Cassini ISS data. The boundaries of the thermal and color anomalies appear to be nearly identical, although the apex of the thermal anomaly appears sharper.

The maximum electron energy flux bombarding Tethys is nearly six times lower than that on Mimas and is constrained to a smaller latitudinal extent, consistent with the relative amplitude and shape of the thermal anomaly on the two bodies [Paranicas et al. 2012; Schenk et al. 2011]. The discovery of Tethys' thermal anomaly, which has a boundary corresponding to an 18 GeV cm 2 s 1 electron flux (compared to 56 GeV cm 2 s 1 on Mimas), greatly strengthens the case that energetic electrons are able to significantly alter an icy satellite surface, and also proves that the threshold electron energy flux able to do so is lower than previously thought. A lower energy flux threshold increases the probability that such alteration occurs on other satellite surfaces. Why high-energy electron bombardment would decrease the IR/UV surface color ratio and why the thermal anomalous region appears darker in visible light images of Tethys, but not on Mimas, remains a mystery.

**Table IcySats-2. Thermal properties of the moons.**

| Target | Bolometric | Thermal Inertia (MKS) | Skindepth (cm) | References |
|---|---|---|---|---|
| **Jovian satellites** | | | | |
| Io | 0.52 | 70 | 0.39[c] | Rathbun et al. [2003] |
| Europa | 0.55 | 70<br>14 ±5 | 0.55[c]<br>0.01[d] | Spencer et al. [1999]<br>Hansen [1973] |
| Ganymede | 0.32 ±0.04 | 70 ±20<br>12 ±3<br>14 ±3 | 0.78[c]<br>0.01[d]<br>0.01[d] | Spencer [1987]<br>Hansen [1973]<br>Morrison and Cruikshank [1973] |
| Callisto | 0.2 ±0.4 | 50 ±10<br>10 ±1 | 0.86[c]<br>0.01[d] | Spencer [1987]<br>Morrison and Cruikshank [1973] |
| **Saturnian satellites** | | | | |
| Mimas | $0.49^{+0.05}_{-0.14}$ | $19^{+57}_{-9}$ | 0.54 | |
| Enceladus | 0.81 ±0.04 | $15^{+24}_{-9}$ | 0.51 | |
| Tethys | 0.67 ±0.11 | $9^{+10}_{-4}$ | 0.36 | |
| Dione | 0.63 ±0.15 | $11^{+18}_{-6}$ | 0.53 | |

**Table ICYSATS-2. Thermal properties of the moons.**

| Target | Bolometric | Thermal Inertia (MKS) | Skindepth (cm) | References |
|---|---|---|---|---|
| Rhea trailing | $0.57^{+0.20}_{-0.26}$ | $8^{+12}_{-5}$ | 0.50 | |
| Rhea leading | $0.63^{+0.11}_{-0.12}$ | $9^{+9}_{-5}$ | 0.56 | |
| Iapetus trailing | $0.31^{+0.15}_{-0.17}$ | $20^{+13}_{-8}$ | 5.22 | |
| Iapetus leading | 0.10[a] | $14^{+7^{a}}_{-8}$ | 3.66 | |
| Phoebe | 0.1 | 20/25[b] | | |

## Dione (IN1c)

The Cassini spacecraft executed five targeted flybys of Dione, passing as close as 500 km to its surface. Three of the flybys were devoted to gravity analysis, designed to understand the interior state of the moon and whether it harbors a subsurface ocean. Such an ocean was inferred from two separate studies: Beuthe et al. [2016] and Hemingway et al. [2016]. Further evidence for a subsurface ocean on Dione, at least at some point, was provided by a geophysical analysis of the formation of Janiculum Dorsae, a raised feature on Dione's surface. The heat flux required to form this feature is 25–60 mW/m$^2$, much greater than that expected solely from radioactive decay, but which can be generated by tidal heating in a liquid ocean [Hammond et al. 2013]. The evidence for an ocean provides the backdrop to the many lines of evidence for residual geologic activity on Dione.

Another intriguing result was the detection on December 15, 2004, of a transient aura-like ring around Dione at 2.65 μm that suggested the existence of an atmosphere [Clark et al. 2008]. Magnetometer data obtained on October 11, 2005, show a weak field perturbation in the upstream region, indicating a tenuous atmosphere [Simon et al. 2011]. The signature was not seen on April 7, 2010. Observing with CAPS, Tokar et al. [2012] discovered a thin atmosphere (~0.01–0.09 particles/cm$^3$) of $O_2^+$ during the close (500 km) flyby on April 7, 2010. A search for forward scattered radiation at solar phase angles > 150°, indicating a plume, was negative [Buratti et al. 2011]. Perhaps the most compelling evidence is the existence of possible cryovolcanic features on Dione. Figure ICYSATS-4 shows an image that includes linear groves and scarps that may be nascent or fossilized activity. Near the center of the image there is an anomalous crater pair that may be a possible volcanic vent. Furthermore, the surrounding area is smooth and relatively crater-free, as if covered by a volcanic deposit. A nearby rampart crater and evidence for amorphous ice suggesting rapid freezing [Newman et al. 2009] also imply some perhaps localized liquid water, although we have previously noted that inferring the existence of amorphous ice is difficult because of the dearth of laboratory data.

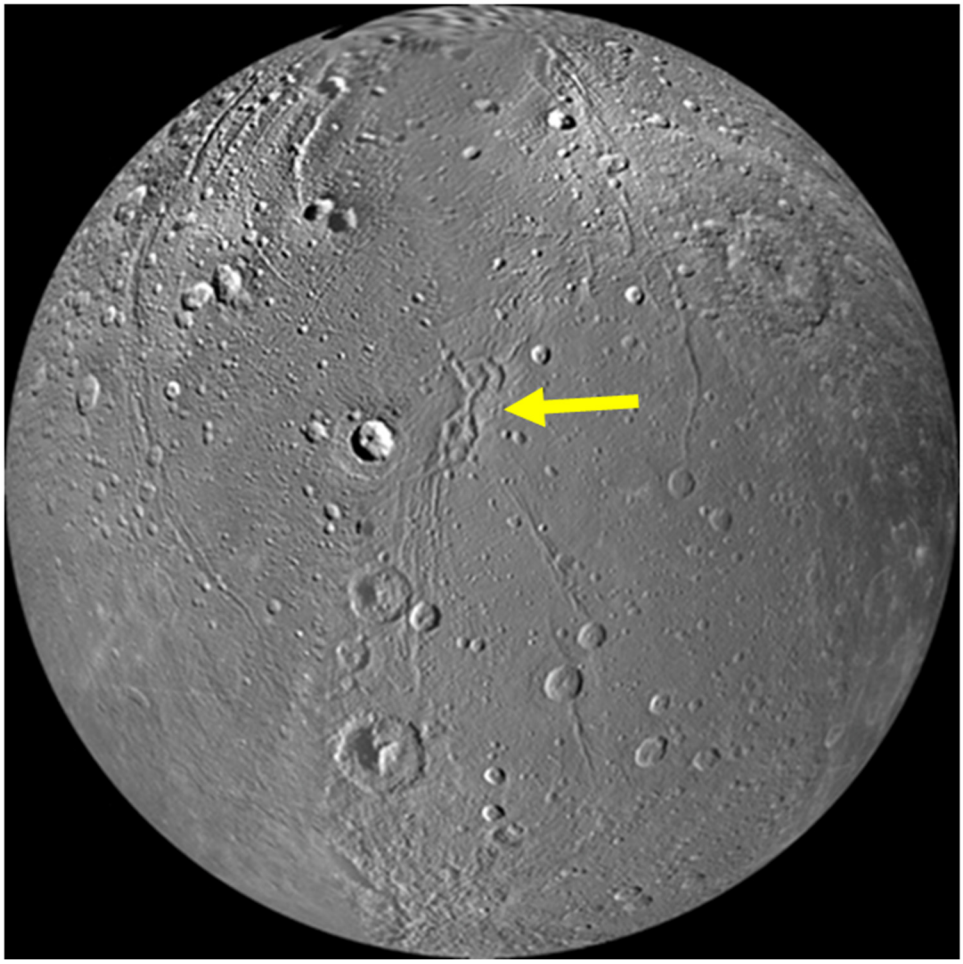

**Figure ICYSATS-4. Possible cryovolcanic features on Dione.**

High phase angle observations of Dione and Tethys were sought during the last year of the mission. Analysis of these data failed to detect any evidence for a plume or atmosphere on either body [Hansen et al. 2018; Buratti et al. 2018a]. No thermal signatures were detected either [Schenk et al. 2018]. The atmosphere appears to be transient, as it was seen only one time. Perhaps there is some type of low-level residual activity on Dione that is sporadic in nature. In any case, possible activity on Dione is one of the truly cold cases of the Cassini mission that will be reopened by future missions.

## Rhea (IN2a)

The largest of the bright ray craters found in the Saturn system, Inktomi (Ø = 49 km), is a flat-floored crater on Rhea with a ray system radiating several hundred kilometers from the crater rim. It was imaged by ISS in August 2007 in three colors at resolutions up to 32 m/pxl and in stereo. The images are the best for a pristine crater in the Saturnian system and reveal a rugged landscape. Most of the ejecta and floor is essentially free of small craters [Wagner et al. 2011; Schenk et al.

2018]. Many of the tectonic lineaments are normal faults and graben, see for example, Wagner et al. [2010, 2007]. Most of this is concentrated in the trailing hemisphere as two major rift zones (Galunlati and Yasmi Chasmata) that trend roughly northeast–southwest and that are up to 3 km deep. These rifts are morphologically similar to those on Dione.

The blue pearls (bluish spots discovered with ISS in Figure ICYSATS-5) are a series of near-IR dark irregular patches located at the crests of the highest ridges or massifs located along the equator of Rhea. Their origin is speculated to be related to infalling or collapse of a former orbiting debris ring [Schenk et al. 2011]. A dedicated search with ISS showed that present Rhea has no ring system [Tiscareno et al. 2010]. The blue pearls are not associated with any tectonic feature along its length or in near proximity. Instead, they appear to be associated with steep slopes (e.g., crater rims). The lack of any constructional artifacts associated with these color patterns on Rhea implies that they are due to regolith disruption [Schenk et al. 2011].

Wispy streaks seen by Voyager on Dione and Rhea are fracture networks [Schenk et al. 2018].

## Tethys (IN2b)

Rugged topography of overlapping craters is typical for wide parts of Tethys [Schenk et al. 2018]. The large 425-km wide impact basin Odysseus is one of the largest well-preserved basins in the Saturnian system. Flat-floor deposits (as commonly found in large craters on the Moon and Mercury) are lacking, suggesting that impact melt ponding did not occur in large quantities. This lack of large melt sheets is characteristic of all craters in the Saturn system [Schenk et al. 2018]. Ithaca Chasma is the dominant tectonic feature. It is a giant rift zone already identified by Voyager, 1,800 km in length and subtending at least 270° of arc, between 70 km and 110 km in width, and 2–5 km deep. It predates the Odysseus basin and thus should not have been formed by this impact feature [Giese et al. 2007].

Red streaks were only found on Tethys and are very enigmatic (Figure ICYSATS-5). They show an enhanced color signature in the near-IR which is a very unusual color for features on Saturn's icy satellites. No associated surface deformation is visible even at image resolutions of 60 m/pxl [Schenk et al. 2015]. The infrared shows distinct compositional changes between the red streaks and the surrounding regions [Buratti et al. 2017].

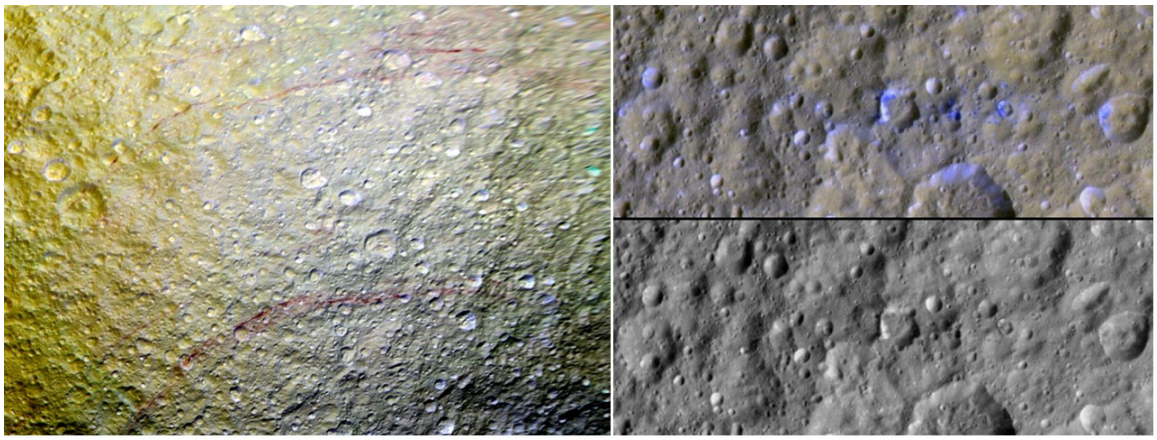

**Figure ICYSATS-5. Red streaks on Tethys (left) and blue pearls on Rhea (right).**

Tethys' equatorial albedo band, first seen in Voyager images, was analyzed in several ISS NAC wavelengths. The band is symmetric 15° on either side of the equator and extends from 0° to 160° W; that is, almost centered on the leading edge of Tethys. There is no evidence that the band is topographically-based; margins are gradational and there is no visible difference in underlying geology [Elder et al. 2007]. ISS NAC polarization images found no evidence for surface textural variations on size-scales comparable to individual geological features (like crater walls and floors on these size scales, the surface texture of Tethys appears to be uniform). However, a banded pattern on the surface was found and that likely originates in the subtle albedo variations tied to Tethys' equatorial band [Elder et al. 2007] and thermally anomalous terrain [Helfenstein et al. 2005].

## Satellite Interiors (IN2c)

Multiple close targeted flybys of the icy moons afforded by an orbital mission as opposed to the single flybys of the Voyager spacecraft provided key data for interior studies. Furthermore, several flybys of Enceladus, Dione, and Rhea were devoted primarily to gravity studies, in which articulations of the spacecraft by reaction wheels or thrusters were avoided. Cassini gravity and imaging experiments teamed up to produce both clear discoveries of internal oceans and interesting mysteries. It appears that multiple Saturnian satellites are well out of hydrostatic equilibrium, reflecting a lack of substantial heat sources and perhaps suggestive of a collisionally dominated history after initial accretion. Rhea is one of these objects, and the gravity data are consistent with a completely undifferentiated body [Tortora et al. 2016]. The lack of evidence for substantial silicates in the surface materials has led to models in which some small amount of differentiation has occurred; however, this is an unstable situation that is difficult to sustain and instead one might look to mechanisms for coating the surface with icy material that obscures a silicate signature.

Cassini data on Mimas and Dione has been interpreted as indicating oceans deep beneath the surfaces of both. For the former, imaging measurements of the moon's unexpectedly large libration imply either a decoupled outer shell (hence, an ocean) or a strongly nonhydrostatic interior

with, for example, an elongated core [Tajeddine et al. 2014]. In the case of Dione, gravity data have been interpreted in terms of a deep ocean via two separate analyses as presented in Beuthe et al. [2016] and Hemingway et al. [2016], but the latter also implies a strongly non-hydrostatic interior. Reconciling these surprising results with models of satellite origin and thermal evolution will be challenging.

The ocean of Enceladus is well-established [Iess et al. 2014; McKinnon 2015; Thomas et al. 2016], but its power source and longevity remain hot topics. Likewise does the question of life, which if present, will (from the point of view of an interiors modeling purist) affect the interpretation of the mass spectrometric data in terms of core-ocean hydrothermal and chemical evolutionary processes.

Iapetus, if in hydrostatic equilibrium, has a shape inconsistent with its present-day spin. This has been interpreted as indicative of a thermal history in which the deep interior was kept hot and dissipative for tidal braking while a thick cold lithosphere retains the shape. If the heat source responsible was short-lived radioactive isotopes, a formation time (since condensation of the first meteorite components) for Iapetus can be derived [Castillo-Rogez et al. 2009]. However, subsequent work revealed that the answer may be very sensitive to ice rheology [Castillo-Rogez et al. 2011], and explanations for the presence of the equatorial ridge in terms of collision with another object [Levison et al. 2011] would severely modify the rotational evolution story.

In contrast with the Jovian system, the intermediate satellite system of Saturn contains objects whose origins and histories, expressed by their interior and surface states, seemed to have been dominated by stochastic events rather than by position relative to their parent planet. Why this is so remains one of the most enduring cold cases left behind by Cassini.

## Small Moons (IN2d)

Table IcySats-3 summarizes our current knowledge of the inner small moons of Saturn.

**Table IcySats-3. Sizes and mean densities of small Saturnian satellites. Table from Buratti et al. [2018b] and Thomas et al. [2007].**

| Object | a, km | b, km | c, km | Rm, km | density, kgm$^{-3}$ | gravity, cms$^{-2}$ |
|---|---|---|---|---|---|---|
| Pan | 17.3 ±0.2 | 14.1 ±0.2 | 10.5 ±0.7 | 13.7 ±0.3 | 400 ±32 | 0.2–1.7 |
| Daphnis | 4.9 ±0.3 | 4.2 ±0.8 | 2.8 ±0.6 | 3.9 ±0.5 | 274 ±142 | 0.0–0.4 |
| Atlas | 20.4 ±0.1 | 17.7 ±0.2 | 9.3 ±0.3 | 14.9 ±0.2 | 412 ±19 | 0.0–1.7 |
| Prometheus | 68.5 ±0.5 | 40.5 ±1.4 | 28.1 ±0.4 | 42.8 ±0.7 | 460 ±21 | 0.8–5.8 |
| Pandora | 51.5 ±0.3 | 39.5 ±0.3 | 31.5 ±0.2 | 40.0 ±0.3 | 509 ±12 | 2.0–5.9 |
| Epimetheus | 64.8 ±0.4 | 58.1 ±0.8 | 53.5 ±0.4 | 58.6 ±0.5 | 625 ±16 | 6.6–10.9 |
| Janus | 101.8 ±0.9 | 93.0 ±0.3 | 74.5 ±0.3 | 89.0 ±0.5 | 642 ±10 | 10.9–16.9 |
| Aegaeon | 0.7 ±0.0 | 0.3 ±0.1 | 0.2 ±0.0 | 0.3 ±0.0 | 539 ±140 | 0.001–0.005 |
| Methone | 1.9 ±0.0 | 1.3 ±0.0 | 1.2 ±0.0 | 1.4 ±0.0 | 307 ±30 | 0.1–0.1 |

**Table IcySats-3. Sizes and mean densities of small Saturnian satellites. Table from Buratti et al. [2018b] and Thomas et al. [2007].**

| Object | a, km | b, km | c, km | Rm, km | density, $kgm^{-3}$ | gravity, $cms^{-2}$ |
|---|---|---|---|---|---|---|
| Pallene | 2.9 ±0.4 | 2.1 ±0.3 | 1.8 ±0.3 | 2.2 ±0.3 | 251 ±75 | 0.1–0.2 |
| Telesto | 16.6 ±0.3 | 11.7 ±0.3 | 9.6 ±0.2 | 12.3 ±0.3 | | |
| Calypso | 14.7±0.3 | 9.3 ±0.9 | 6.4 ±0.3 | 9.5 ±0.4 | | |
| Polydeuces | 1.5 ±0.3 | 1.3 ±0.4 | 1.0 ±0.2 | 1.3 ±0.3 | | |
| Helene | 22.6 ±0.2 | 19.6 ±0.3 | 13.3 ±0.2 | 18.1 ±0.2 | | |
| Hyperion | 164.1 ±1.7 | 130.1 ±4.0 | 107.1 ±4.3 | 135.9 ±3.1 | 535 ±37 | 17.3–20.8 |

The low densities of the small inner moons of Saturn, which were refined by the close flybys at the end of the mission, is consistent with accretion from ring material. The new data on the moons embedded in the A-ring show that the color of these moons becomes more similar to the rings the closer they are to Saturn. This result suggests there is an ongoing accretion of a reddish chromophore that may be a mixture of organics, silicates, and iron, onto the surfaces of the rings [Buratti et al. 2017]. The difference in color between the moons and their adjacent ring can be explained by the accretion of bright, icy E-ring particles. In essence, each moon's surface is subjected to a balance between these two ongoing processes, with their distance from Saturn and Enceladus determining the final result (Figure IcySats-6). The detection of abundant ice grains by CDA in the region of these moons supports this view. The bluer core of Atlas is also explained by the accretion of E-ring particles, which have a wider range of inclinations than main ring particles. The finding by MIMI of a dearth of high-energy ions also lessens the competing alteration processes from bombardment by magnetospheric particles. The strong crystalline water ice band at 1.65 μm also suggests the lack of importance of these processes. This low energy environment also renders comparisons with the identity of the red chromophore on the trailing hemispheres of main moons of Saturn, especially Dione and Rhea, problematical, as they dwell in a region where alterations by ions is significant and would tend to darken and redden the surfaces. Finally, contamination of Saturn's rings by bright icy particles diminishes the argument that the observed brightness of the rings bespeaks a recent formation [Zhang et al. 2017].

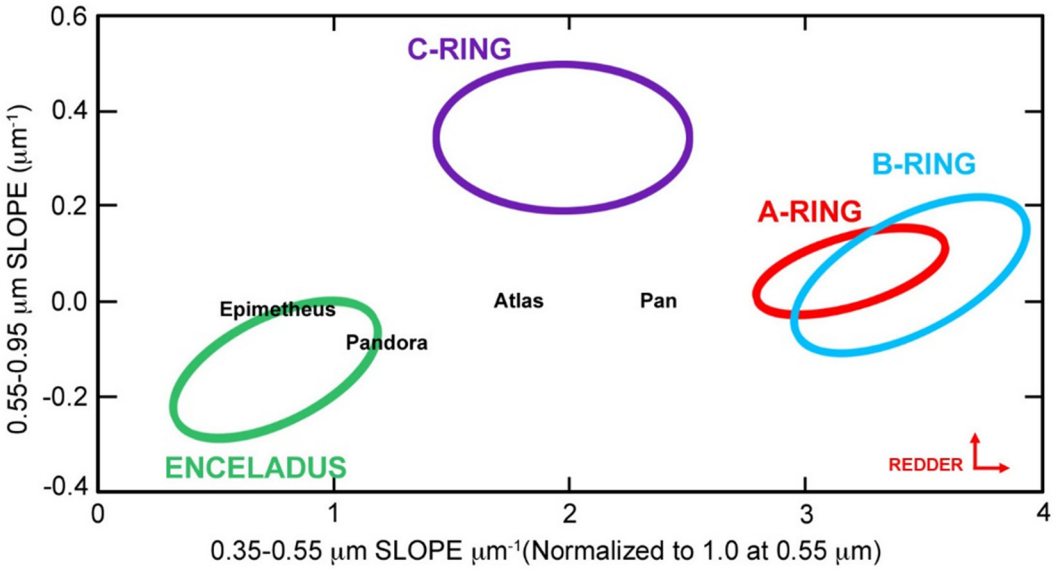


**Figure ICYSATS-6. Colors of the ring moons compared to the rings. Figure based on Filacchione et al. [2013, 2012] and Buratti et al. [2018b].**

The moons record complex geologic histories including groove formation caused by tidal stresses, accretion of ring particles, and possible accretion of debris from impacts on larger moons. The CDA finding of porous surfaces for the ring moons further supports substantial accretion. Although the topography and surface slopes strongly suggest the equatorial ridges of Pan and Atlas are accreted from rings and are not formed by normal surface transport, the variety of forms of ridges on these objects, and the minimal ridges on Daphnis, show that much remains to be understood about their formation and relation to the main rings. The high-resolution images strongly suggest exposures, especially on Epimetheus, Janus, and Pandora, of a solid substrate distinct from the mobile regolith that generally conceals bedrock on small solar system objects. These exposures may eventually help reveal systematic trends of body history and structures for the whole of the Saturn satellite system. The moons Aegaeon, Methone, and Pallene have shapes of equilibrium ellipsoids indicative of weak or mobile surfaces that cannot support shear stresses [Thomas et al. 2013]. These forms are unique for such small objects, usually fractured or clumpy, and as yet are unexplained. An example of ISS, CIRS, and VIMS data on Atlas is shown in Figure ICYSATS-7.

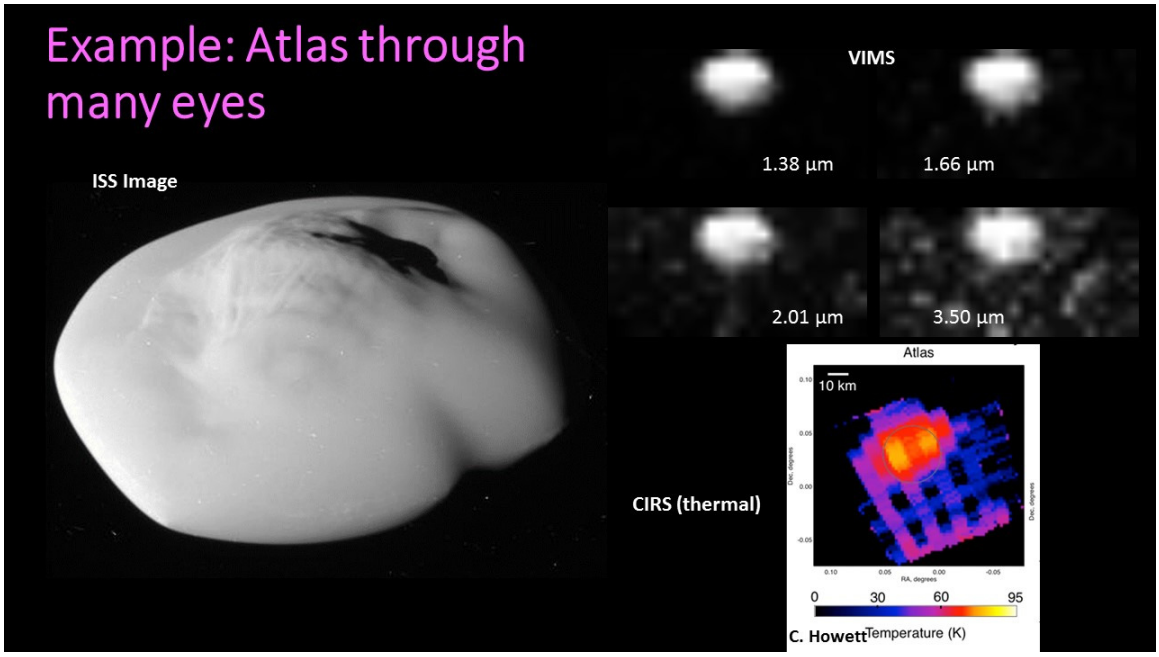


**Figure ICYSATS-7. ISS, VIMS, and CIRS observations of Atlas obtained during the F-ring orbits.**

## Hyperion (IN2e)

The chaotically rotating satellite, Hyperion, has unique sponge-like topography that may reflect sublimation of species more volatile than water ice [Thomas et al. 2007]. The chaotic rotation of Hyperion was analyzed using data from three flybys. The Lyapunov timescale was found to be approximately 100 days [Harbison et al. 2011]. As Iapetus is, Hyperion may be coated with material from the Phoebe ring, but because the moon is in chaotic rotation it is not found preferentially on one hemisphere. Rather, it tends to be located in the bottoms of craters or pits, similar to sun cups on the Earth, in which dark material is concentrated in warmer areas through a process of thermal segregation. This material is rich in organics, including possibly aromatics. The $CO_2$ on the surface is probably combined in some way with water ice. Dalton et al. [2012] identify aromatic and aliphatic hydrocarbons in the low-albedo material, and possibly $H_2$. As for Iapetus and the other moons, nanophase iron is thought to act as a coloring agent [Clark et al. 2012].

## Iapetus (IN2f)

The global and regional topography of Iapetus is much less smooth than for the other mid-sized icy moons [Thomas et al. 2007; Lee et al. 2010]. A total of 10 basins larger than 300 km have been identified on Iapetus (despite the lack of resolved imaging in some locations), but only four on Rhea. Dione, Tethys, and Mimas are similarly depleted [Schenk et al. 2018]. ISS data show numerous impact craters down to the resolution limit [Denk et al. 2010].

Iapetus' global albedo dichotomy, first described by the spacecraft's eponym Jean-Dominique Cassini in 1677 and unexplained since then, has been solved through Cassini CIRS and ISS data [Spencer and Denk 2010]. Dust from Phoebe or possibly from other retrograde-orbiting irregular moons has likely been painting the surface of Iapetus, forming the newly-detected global color dichotomy of Iapetus [Denk et al. 2010], which triggered the evolution of low-latitude and mid-latitude parts of the leading side into the stark bright and dark patterns we see today as the global albedo dichotomy [Spencer and Denk 2010], accentuated with the thermal migration of water ice [Denk et al. 2010]. A major property of the global color dichotomy is that dark material on the leading side is redder than dark material on the trailing side, and that bright material on the leading side (mainly at high latitudes) is also redder than bright material on the trailing side [Denk et al. 2010]. Cassini ISS data showed that the stark dark-bright contrast is also a local phenomenon. The surface is either bright or dark, but almost never gray, even in the transition zone between the dark Cassini Regio and the bright Roncevaux Terra and Saragossa Terra [Denk et al. 2008].

Observations of small, bright-ray craters within the dark terrain indicate that the dark material corresponds to a blanket of a few meters or less in thickness…

Observations of small, bright-ray craters within the dark terrain indicate that the dark material corresponds to a blanket of a few meters or less in thickness [Denk et al. 2010], a finding also supported by Titan Radar Mapper (RADAR) data [Ostro et al. 2006] and consistent with the thermal migration model of Spencer and Denk [2010].

A huge and enigmatic ridge located exactly at the equator was discovered in ISS images [Porco et al. 2005; Denk et al. 2005a; Denk et al. 2005b]. In places, this ridge is up to 20 km high and 70 km across, and it spans almost 75% of the moon's circumference [Porco et al. 2005; Denk et al. 2008; Giese et al. 2008; Singer and McKinnon 2011]. While the ridge is mainly continuous on the leading side (Toledo Montes), it separates into the isolated mountains of the Carcassone Montes which were already discovered in Voyager data (and thus sometimes dubbed Voyager mountains) [Denk et al. 2000]. In general, it shows a wide range of cross-sections and heights at different longitudes [Denk et al. 2008; Singer et al. 2012]. Singer and McKinnon [2011] did not find potential hints for tectonic or volcanic origin. Defying any obvious explanation, numerous endogenic and exogenic formation mechanisms were proposed, for example, see short review of them by Damptz et al. [2018]. None of them can be favored over the others at this point.

$CO_2$ was found on Iapetus during an untargeted flyby just prior to the Huygens probe separation [Buratti et al. 2005], and spectra with km-scale resolution were obtained during a targeted flyby on September 10, 2007. Clark et al. [2012] identified additional key components of the surface of Iapetus in addition to $CO_2$ and $H_2O$, including bound water, $H_2$, OH-bearing minerals, trace organics, and possibly ammonia. The $CO_2$ on Iapetus was enriched in the low-albedo areas, reaching a maximum at the apex of motion where the albedo is lowest. The Clark et al. [2012] posits the presence of nanophase metallic iron particles and an iron oxide, probably hematite to contribute to the observed Rayleigh scattering peak in the visible part of the spectrum. Figure ICYSATS-8 is a summary of the features in the spectrum of Iapetus.

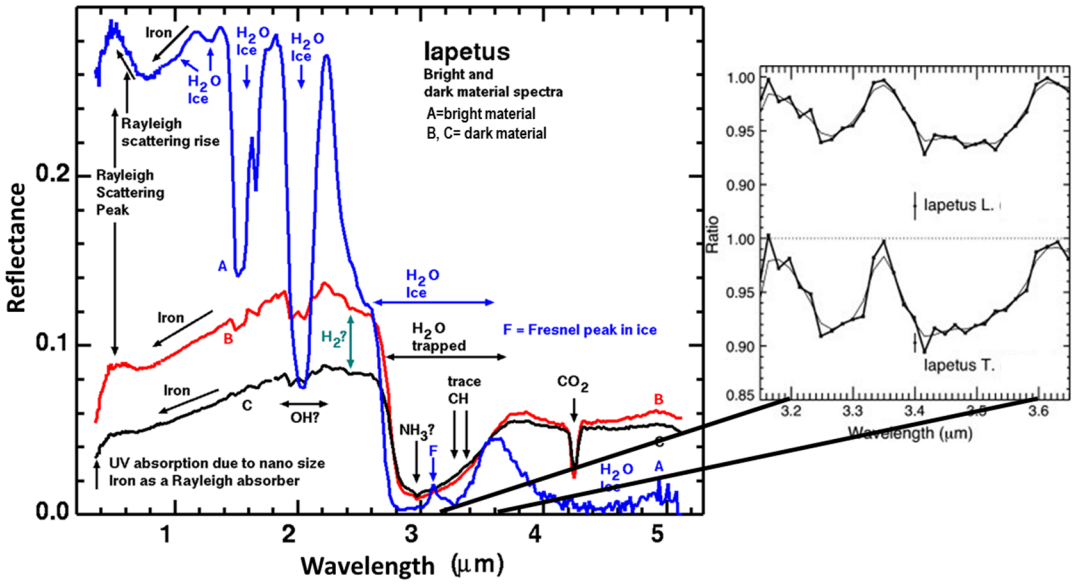


**Figure ICYSATS-8. The spectrum of Iapetus showing explanations for the spectral lines of the bright material and two examples of dark material on Iapetus. *B = dark material:* The identification of aromatic hydrocarbons in the spectrum. This graph gives the residuals that result from a best-fit Hapke compositional model to the leading and trailing sides. Absorption bands at 3.28 μm are characteristic of aromatic hydrocarbons, while those between 3.35 and 3.6 μm are characteristic of aliphatic hydrocarbons. *A = bright material:* is based on Clark et al. [2012] and *B = dark material:* is based on Cruikshank et al. [2014].**

An analysis of the 2.7 to 4.0 μm spectral region by Cruikshank et al. [2010, 2014] identified the presence of both aromatic and aliphatic hydrocarbons in the dark material on Iapetus. The aromatic band near the CH stretching modes of aromatic hydrocarbons at ~3.28 μm is especially strong, and is likely due to aromatic hydrocarbons. Because surfaces rich in aromatic hydrocarbons are readily carbonized via UV radiation, these substances are not stable on the surface of Iapetus, and thus the process of accretion of Phoebe ring particles must be ongoing.

The dark material on Iapetus is abundant enough to perform compositional modeling. The 3-micron-bound water band was found to match hydrated iron oxides [Clark et al. 2012] and subsequent recalibration of VIMS [Clark et al. 2018] show that spectra of the dark materials also shows a 1.9-micron water absorption that matches hydrated iron oxides. The linear slope, blue peak, and absorption shorter than 0.5 microns, argue for space-weathered silicates (thus nano-metallic iron) as the explanation of the UV-visible spectrum. The lack of any hint of absorptions from tholins in the IR is enough abundance to explain the UV-visible spectrum, and argues for the space-weathered silicates and iron oxide explanation [Clark et al. 2012].

Clark et al. [2012] also explained that the differences in color between the Iapetus dark material and Phoebe is simply due to abundance differences of space-weathered silicates, hydrated iron oxides, and ice. According to this model, the flatter, grayer spectrum of Phoebe compared to Iapetus dark material is due to lower abundance of the iron oxides and space-weathered silicates.

## Other Icy Satellites Science not in CSM

Phoebe was the first targeted flyby on June 11, 2004. Its global shape is close to an oblate spheroid, with a = b to within the uncertainties of the data [Thomas 2010; Castillo-Rogez et al. 2012]. Its mean radius is 106.4 ±0.4 km and its mean density is 1.64. This high density along with its compositional differences with the mid-sized regular satellites of Saturn, support the evidence that it is a captured body [Johnson and Lunine 2005b]. Numerous impact craters are visible on the surface; they range in diameter from the lower limit imposed by the ISS image resolution up to ≈100 km [Porco et al. 2005]. Phoebe's topography, relative to an equipotential surface, is within the range of other small objects and is much higher than that for clearly relaxed objects [Thomas 2010]. Digital Terrain Model (DTM) and orthoimage of the surface were produced from ISS data [Giese et al. 2006]. The J2000 spin-axis was found at Dec = 78.0° ±0.1°; RA = 356.6° ±0.3°, substantially different from the former Voyager solution [Giese et al. 2006]. Finally, Phoebe dust ring, discovered from Earth, has also been observed with the ISS Wide Angle Camera [Tamayo et al. 2014].

Mimas was the least studied of the main moons, with no targeted flyby.

Mimas was the least studied of the main moons, with no targeted flyby. The best images obtained at this flyby have a spatial resolution of ~93 m/pxl. There is morphologic evidence for a highly degraded impact basin of ~153 km diameter, northeast of crater Herschel [Schmedemann and Neukum 2011].

All irregular moons except Phoebe were discovered between year 2000 and 2007. Since this was after the launch of Cassini-Huygens, they were not part of the original science goals. Therefore, a dedicated observation campaign with ISS was initiated for the Solstice mission. ISS observed 25 of Saturn's 38 known irregular moons, and precise rotational periods could be derived for most of them. The light curves are indicative for objects with quite different shapes. The rotational periods vary between 5.45 h and 76.13 h. Many asteroids of similar size rotate faster; this indicates that Saturn's irregular moons have rather low densities. Some objects show very distinct 3 maxima/3 minima light curves with an equal spacing of the extrema. Convex-shape models of these moons resemble triangular prisms, but they might actually be contact-binary objects. Other light curves show patterns that might even hint to binary moons. It is likely that non-random correlations were found between the ranges to Saturn, the orbit directions, orbit tilts, object sizes, and the rotation periods. The physical cause, especially for size and spin relations to orbital elements, is unknown at this point. For further reading, we refer to Denk et al. [2018] or Denk and Mottola [2013, 2014].

## Open Questions for Icy Satellite Science

The top open questions for icy moon science, as compiled by the Cassini ISWG meeting in March 2018 and compiled in a peer-reviewed paper by Buratti et al. [2017], are:

1. What are some of the minor constituents of the Saturnian moons, and are they endogenic or exogenic? If exogenic, is the accretional process still ongoing?

2. Can the D/H ratio be measured on these moons? If so, how does it compare with that of other regions of the Solar System, and what does that imply about the transport of volatiles on a large scale? Clark et al. [2019] derives the D/H in the ice on the satellites and rings and the 12C/13C on the carbon dioxide. The D/H is similar to terrestrial values for the satellites and rings except for Phoebe, where deuterium and C13 are high.

3. Is ammonia hydrate on the surfaces of any of the moons?

4. What is the identity of the red chromophore on these bodies' surfaces? Is it nano-iron or organic material, and what are the transport processes to move this material around the Solar System? Is it the same chromophore that exists in the main ring system?

5. What is the total heat production on Enceladus; how and why does it vary? What does this imply about the cause of activity on the moon? Why is only the South Pole active and not the North Pole (what is Enceladus' tectonic history)? What is the nature of the plumbing that connects the ocean to the surface? Is there any evidence for seasonal variations in output? Is there life in Enceladus' ocean?

6. Is there residual activity on Dione and Tethys, and if so, what does this imply about their recent history? Are the red streaks on Tethys evidence for such activity?

7. What caused the ridge on Iapetus? Is it evidence for a past ring? Did other moons have rings in the past?

8. Why does the origin of the moons of Jupiter and Saturn seem to diverge, with the Jovian moons being formed relative to their position from Jupiter, and the Saturnian moons being formed by stochastic events?

9. Why are some of the moons not in hydrostatic equilibrium? Rhea and Dione, incompletely, for example.

10. To what extent do magnetospheric particles alter the optical properties of the moons? Does contamination by ring particles, including those from the E-ring, dominate this process?

11. What are the blue pearls on Rhea?

## Earth (Moon)

From Clark [2009]:

> "Data from the Visual and Infrared Mapping Spectrometer (VIMS) on Cassini during its flyby of the Moon in 1999 show a broad absorption at 3 micrometers due to adsorbed water and near 2.8 micrometers attributed to hydroxyl in the sunlit surface on the Moon. The amounts of water indicated in the spectra depend on the type of mixing and the grain sizes in the rocks and soils but could be 10 to 1000 parts per million and locally higher. Water in the Polar Regions may be water that has migrated to the colder environments there. Trace hydroxyl is observed in the anorthositic highlands at lower latitudes."

## Jupiter (Galilean Satellites)

In December 2000, Cassini flew by Jupiter for a gravity assist to Saturn. The geometry of the flyby was set by the trajectory requirements for Saturn so most of the moons were quite distant, however, several significant new results were obtained. Brown et al. [2003] documents VIMS results from the Jupiter flyby: VIMS documented a surprisingly high opposition surge on Europa, and the first visual-near-IR spectra of Himalia. UVIS observed Europa's $O_2$ atmosphere. ISS studied Io's volcanic activity.

### *Io*

Io was observed during four eclipses. ISS imaged the glow of Io's ambient atmosphere from the K, Na, O, $S_2$, and $SO_2$ coming from its volcanoes. Differences in the altitude of the emissions indicate stratification of the Io atmosphere [Geissler et al. 2004].

### *Europa*

VIMS data provided the first near-IR phase curve of Europa [Simonelli and Buratti 2004]. Europa exhibits a remarkable surge in brightness (~0.2 mag/deg) under 1°, comparable to the lunar opposition surge measured by Clementine [Buratti et al. 1996]. Furthermore, data at small phase angles show a clear trend with albedo, such that wavelengths corresponding to higher albedos have smaller surges, consistent with shadow illumination. The VIMS results suggest that neither CBE nor shadow hiding provide a complete description of Europa's opposition surge below 1° [Brown et al. 2003].

UVIS observed emissions from Europa's $O_2$ atmosphere and mapped its spatial extent. Atomic oxygen extends further from Europa than $O_2$, however, it does not form a torus [Hansen et al. 2005]. Analysis of other emissions from other neutrals and ions near Europa constrains the level of eruptive activity and suggests that it can only be intermittent—no plumes comparable to Enceladus were active at the time of the Cassini flyby [Shemansky et al. 2014].

## Galilean moons

VIMS spectra of the Galilean satellites confirmed the spectral features in the Galileo Near-Infrared Mapping Spectrometer Subsystem (NIMS) data. Brown et al. [2003] also noted similar spectral structure as in NIMS data attributed to a CN bond near 4.5 microns. This structure was also seen in VIMS data of the Saturnian satellites, see for example, Clark et al. [2005, 2008], but was later found to be due to a calibration error [Clark et al. 2012].

## Himalia

The disk of Himalia was resolved in ISS images, and show that it is not spherical [Porco et al. 2003]. If principal axes were visible, the diameters are 150 ±10 km × 120 ±5 km. VIMS data shows that Himalia has a slightly reddish spectrum, an apparent absorption near 3 μm, and a geometric albedo of 0.06 ±0.01 at 2.2 μm (assuming an average 85-km radius). If the 3-μm feature in Himalia's spectrum is eventually confirmed, it would be suggestive of the presence of water in some form, either free, bound, or incorporated in layer-lattice silicates [Brown et al. 2003].

# ACRONYMS

*Note: For a complete list of Acronyms, refer to Cassini Acronyms – Attachment A.*

| | |
|---|---|
| AO | Announcement of Opportunity |
| CAPS | Cassini Plasma Spectrometer |
| CDA | Cosmic Dust Analyzer |
| CIRS | Composite Infrared Spectrometer |
| CSM | Cassini Solstice Mission |
| D/H | Deuterium to Hydrogen |
| DTM | Digital Terrain Model |
| DWG | Discipline Working Group |
| FRPO | F-ring and Proximal Orbits |
| FUV | far ultraviolet |
| INMS | Ion and Neutral Mass Spectrometer |
| IR | infrared |
| ISS | Imaging Science Subsystem |
| ISWG | Icy Satellites Working Group |
| KBO | Kuiper Belt object |
| LEMMS | Low Energy Magenotospheric Measurement System |
| MAPS | Magnetospheres and Plasma Science |
| MIMI | Magnetospheric Imaging Instrument |
| NAC | narrow angle camera |
| NIMS | Near Infrared Mapping Spectrometer Subsystem |
| PDS | Planetary Data System |
| RADAR | Titan Radar Mapper |
| SOST | Satellites Orbiter Science Team |
| TM | Traceability Matrix |
| UV | ultraviolet |
| UVIS | Ultraviolet Imaging Spectrograph |
| VIMS | Visual and Infrared Imaging Spectrometer |

## REFERENCES

*Disclaimer: The partial list of references below correspond with in-text references indicated in this report. For all other Cassini references, refer to Attachment B – References & Bibliographies; Attachment C – Cassini Science Bibliographies; the sections entitled References contributed by individual Cassini instrument and discipline teams located in Volume 1 Sections 3.1 and 3.2 Science Results; and other resources outside of the Cassini Final Mission Report.*

Behounkova, M., G. Tobie, O. Cadek, G. Choblet, C. Porco, F. Nimmo, (2015), Timing of water plume eruptions on Enceladus explained by interior viscosity structure, Nature Geoscience 8, 8, 601–604, doi: 10.1038/ngeo2475.

Beuthe, M., A. Rivoldini, A. Trinh, (2016), Enceladus's and Dione's floating ice shells supported by minimum stress isostasy, Geophysical Research Letters 43, 19.

Black, G. J., D. B. Campbell, L. M. Carter, (2007), Arecibo radar observations of Rhea, Dione, Tethys, and Enceladus, Icarus 191, 2, 702–11, doi: 10.1016/j.icarus.2007.06.009.

Black, G. J., D. B. Campbell, L. M. Carter, S. J. Ostro, (2004), Radar detection of Iapetus. Science 304, 5670, 553–553.

Bouquet, A., O. Mousis, J. H. Waite, S. Picaud, (2015), Possible evidence for a methane source in Enceladus' ocean, Geophysical Research Letters 42, 5, 1334–1339, doi: 10.1002/2014GL063013.

Brown, R. H., R. N. Clark, B. J. Buratti, D. P. Cruikshank, J. W. Barnes, R. M. E. Mastrapa, J. Bauer, S. Newman, T. Momary, K. H. Baines, G. Bellucci, F. Capaccioni, P. Cerroni, M. Combes, A. Coradini, P. Drossart, V. Formisano, R. Jaumann, Y. Langevin, D. L. Matson, T. B. McCord, R. M. Nelson, P. D. Nicholson, B. Sicardy, C. Sotin, (2006), Composition and physical properties of Enceladus' surface, Science 311, 5766, 1425–1428. doi: 10.1126/science.1121031.

Brown, R. H., K. H. Baines, G. Bellucci, J. P. Bibring, B. J. Buratti, F. Capaccioni, P. Cerroni, R. N. Clark, A. Coradini, D. P. Cruikshank, P. Drossart, V. Formisano, R. Jaumann, Y. Langevin, D. L. Matson, T. B. McCord, V. Mennella, R. M. Nelson, P. D. Nicholson, B. Sicardy, C. Sotin, S. Amici, M. A., Chamberlain, G. Filacchione, G. Hansen, K. Hibbitts, M. Showalter, (2003), Observations with the Visual and Infrared Mapping spectrometer (VIMS) during Cassini's flyby of Jupiter, Icarus, 164, 2, 461–470. doi: 10.1016/s0019-1035(03)00134-9.

Buratti, B. J. et al., (2018a), First Results from Cassini's Five Fabulous Flybys of Saturn's Ring Moons, Science, revision submitted May 25, 2018.

Buratti, B. J., P. C. Thomas, E. Roussos, C. Howett, M. Seiss, A. R. Hendrix, P. Helfenstein, R. H. Brown, R. N. Clark, T. Denk, G. Filacchione, H. Hoffmann, G. H. Jones, H. Khawaja, P. Kollman, N. Krupp, J. Lunine, T. S. Momary, C. Paranicas, F. Postberg, M. Sachse, F. Spahn, J. Spencer, R. Srama, T. Albin, K. H. Baines, M. Ciarniello, T. Economou, S. Hsu, S. Kempf, S. M. Krimigis, D. Mitchell, G. Moragas-Klostermeyer, P. D. Nicholson, C. C. Porco,

H. Rosenberg, J. Simolka, L. A. Soderblom, (2018b), First Results from Cassini's Flybys of Saturn's Ring Moons at the End of Mission, Science, submitted.

Buratti, B. J., R. N. Clark, F. Crary, C. J., Hansen, A. R. Hendrix, C. J. A. Howett, J. Lunine, C. Paranicas, (2017), Cold cases: What we don't know about Saturn's Moons, Planetary and Space Science, 155, 41–49.

Buratti, B. J., S. P. Faulk, J. A. Mosher, K. H. Baines, R. H. Brown, R. N. Clark, P. D. Nicholson, (2011), Search for and limits on plume activity on Mimas, Tethys, and Dione with the Cassini Visual Infrared Mapping Spectrometer (VIMS), Icarus 214, 2, 534–540. doi: 10.1016/j.icarus.2011.04.030.

Buratti, B. J., D. P. Cruikshank, R. H. Brown, R. N. Clark, J. M. Bauer, R. Jaumann, T. B. McCord, D. P. Simonelli, C. A. Hibbitts, G. B. Hansen, T. C. Owen, K. H. Baines, G. Bellucci, J. P. Bibring, F. Capaccioni, P. Cerroni, A. Coradini, P. Drossart, V. Formisano, Y. Langevin, D. L. Matson, V. Mennella, R. M. Nelson, P. D. Nicholson, B. Sicardy, C. Sotin, T. L. Roush, K. Soderlund, A. Muradyan, (2005), Cassini Visual and Infrared Mapping Spectrometer observations of Iapetus: detection of CO2, Astrophysical Journal Letters, 622, 2, 149–52.

Buratti, B. J., J. K. Hillier, M. Wang, (1996), The lunar opposition surge: Observations by Clementine, Icarus, 124, 2, 490–499.

Buratti, B. J., J. A. Mosher, T. V. Johnson, (1990), Albedo and color maps of the saturnian satellites, Icarus, 87, 2, 339–357.

Buratti, B. and J. Veverka, (1984), Voyager photometry of Rhea, Dione, Tethys, Enceladus and Mimas, Icarus, 58, 2, 254–264.

Burch, J. L., J. Goldstein, W. S. Lewis, D. T. Young, A. J. Coates, M. K. Dougherty, N. Andre, (2007), Tethys and Dione as sources of outward-flowing plasma in Saturn's magnetosphere, Nature 447, 7146, 833–835. doi: 10.1038/nature05906.

Castillo-Rogez, J. C., D. Hemingway, W. B. McKinnon, G. Schubert, G. Tobie, (2018), Origin and Evolution of Saturn's Midsize Moons, Part 3: Saturn's Icy Moons, In Enceladus and the icy moons of Saturn, (eds.) P. M. Schenk, R. N. Clark, C. J. A. Howett, A. J. Verbiscer, J. H. Waite, The University of Arizona Press, Tucson, AZ.

Castillo-Rogez, J. C., T. V. Johnson, P. C. Thomas, M. Choukroun, D. L. Matson, J. I. Lunine, (2012), Geophysical evolution of Saturn's satellite Phoebe, a large planetesimal in the outer Solar System, Icarus, 219, 1, 86–109, doi: 10.1016/j.icarus.2012.02.002.

Castillo-Rogez, J. C., M. Efroimsky, V. Lainey, (2011), The tidal history of Iapetus: Spin dynamics in the light of a refined dissipation model, Journal of Geophysical Research: Planets, 116, E9.

Castillo-Rogez, J., T. V. Johnson, M. H. Lee, N. J. Turner, D. L. Matson, J. Lunine, (2009), Al-26 decay: Heat production and a revised age for Iapetus, Icarus, 204, 2, 658–662, doi: 10.1016/j.icarus.2009.07.025.

Clark, R. N., R. H. Brown, D. P. Cruickshank, D. P. Swayze, (2019), Isotopic ratios of Saturn's Rings and Satellites: Implications for the Origin of Water and Phoebe, Icarus, 321, 791–802.

Clark, R. N, R. H. Brown, D. M. Lytle, M. Hedman, (2018), The VIMS wavelength and radiometric calibration 19, Final Report.

Clark, R. N., R. H. Brown, G. A. Swayze, D. P. Cruikshank, (2017a), Detecting isotopic signatures and measuring isotopic ratios on solid icy surfaces: Implications for origin and evolution, American Geophysical Union (AGU) Fall Meeting, abstract P52B-06.

Clark, R. N., R. H. Brown, G. A. Swayze, D. P. Cruikshank, (2017b), Detection of deuterium in icy surfaces and the D/H ratio of icy objects, American Astronomical Society (AAS), Division for Planetary Sciences Meeting, meeting 49, id 210.01.

Clark, R. N., R. H. Brown, D. P. Cruikshank, (2016a), CO2 and 12C: 13C isotopic ratios on Phoebe and Iapetus, American Geophysical Union (AGU) Fall Meeting, abstract P42A-07.

Clark, R. N., R. H. Brown, D. M. Lytle, D. P. Cruikshank, (2016b), Composition of Phoebe and Iapetus: bound water and possible deuterated water, American Astronomical Society (AAS), Division for Planetary Sciences Meeting, meeting 48, id 519.06.

Clark, R. N., D. P. Cruikshank, R. Jaumann, R. H. Brown, K. Stephan, C. M. D. Ore, K. E. Livo, N. Pearson, J. M. Curchin, T. M. Hoefen, B. J. Buratti, G. Filacchione, K. H. Baines, P. D. Nicholson, (2012), The surface composition of Iapetus: Mapping results from Cassini VIMS, Icarus, 218, 2, 831–860. doi: 10.1016/j.icarus.2012.01.008.

Clark, R. N., (2009), Detection of adsorbed water and hydroxyl on the Moon, Science, 326, 5952, 562–564, doi: 10.1126/science.1178105.

Clark, R. N., J. M. Curchin, R. Jaumann, D. P. Cruikshank, R. H. Brown, T. M. Hoefen, K. Stephan, J. M. Moore, B. J. Buratti, K. H. Baines, P. D. Nicholson, R. M. Nelson, (2008), Compositional mapping of Saturn's satellite Dione with Cassini VIMS and implications of dark material in the Saturn system, Icarus, 193, 2, 372–386.

Clark, R. N., R. H. Brown, R. Jaumann, D. P. Cruikshank, R. M. Nelson, B. J. Buratti, T. B. McCord, J. Lunine, K. H. Baines, G. Bellucci, J. P. Bibring, F. Capaccioni, P. Cerroni, A. Coradini, V. Formisano, Y. Langevin, D. L. Matson, V. Mennella, P. D. Nicholson, B. Sicardy, C. Sotin, T. M. Hoefen, J. M. Curchin, G. Hansen, K. Hibbits, K. D. Matz, (2005), Compositional maps of Saturn's moon Phoebe from imaging spectroscopy, Nature, 435 7038, 66–69, doi: 10.1038/nature03558.

Collins, G. C. and J. C. Goodman, (2007), Enceladus' south polar sea, Icarus, 189, 1, 72–82.

Cruikshank, D. P., C. M. D. Ore, R. N. Clark, Y. J. Pendleton, (2014), Aromatic and aliphatic organic materials on Iapetus: Analysis of Cassini VIMS data, Icarus, 233, 306–315, doi: 10.1016/j.icarus.2014.02.011.

Cruikshank, D. P., A. W. Meyer, R. H. Brown, R. N. Clark, R. Jaumann, K. Stephan, C. A. Hibbitts, S. A. Sandford, R. M. E. Mastrapa, G. Filacchione, C. M. D. Ore, P. D. Nicholson, B. J. Buratti, T. B. McCord, R. M. Nelson, J. B. Dalton, K. H. Baines, D. L. Matsoni, (2010), Carbon dioxide on the satellites of Saturn: Results from the Cassini VIMS investigation and revisions to the VIMS wavelength scale, Icarus, 206, 2, 561–572. doi: 10.1016/j.icarus.2009.07.012.

Dalton III, J. B., D. P. Cruikshank, R. N. Clark, (2012), Compositional analysis of Hyperion with the Cassini Visual and Infrared Mapping Spectrometer, Icarus, 220, 2, 752–776. doi: 10.1016/j.icarus.2012.05.003.

Damptz, A. L., A. J. Dombard, M. R. Kirchoff, (2018), Testing models for the formation of the equatorial ridge on Iapetus via crater counting, Icarus, 302, 134–144. doi: 10.1016/j.icarus.2017.10.049.

Denk, T., S. Mottola, F. Tosi, W. B. Bottke, D. P. Hamilton, (2018), The Irregular Satellites of Saturn, Part 3: Saturn's Icy Moons, In Enceladus and the Icy Moons of Saturn, (eds.) P. M. Schenk, R. N. Clark, C. J. A. Howett, A. J. Verbiscer, J. H. Waite, The University of Arizona Press, Tucson, AZ.

Denk, T. and S. Mottola, (2014), Periods, poles, and shapes of irregular satellites of Saturn from lightcurves, American Astronomical Society (AAS), Division for Planetary Sciences Meeting abstracts 46, id 304.09.

Denk, T. and S. Mottola, (2013), Irregular Saturnian moon lightcurves from Cassini-ISS Observations: Update, 45th American Astronomical Society (AAS), Division for Planetary Sciences Meeting, 6–11 October 2013, Denver, CO, vol. 45, no. 9, p. 170, id 406.08.

Denk, T., G. Neukum, T. Roatsch, C. C. Porco, J. A. Burns, G. G. Galuba, N. Schmedemann, P. Helfenstein, P. C. Thomas, R. J. Wagner, R. A. West, (2010), Iapetus: Unique surface properties and a global color dichotomy from Cassini Imaging, Science, 327, 5964, 435–439, doi: 10.1126/science.1177088.

Denk, T., G. Neukum, N. Schmedemann, T. Roatsch, R. J. Wagner, B. Giese, J. E. Perry, P. Helfenstein, E. P. Turtle, C. C. Porco, (2008), Iapetus imaging during the targeted flyby of the Cassini Spacecraft, 39th Lunar and Planetary Science Conference, League City, TX, 10–14 March 2008.

Denk, T., G. Neukum, T. Roatsch, A. S. McEwen, E. P. Turtle, P. C. Thomas, P. Helfenstein, R. J. Wagner, C. C. Porco, J. E. Perry, (2005a), First imaging results from the Iapetus b/c flyby of the Cassini Spacecraft, NASA Technical Reports Server, Lunar and Planetary Science XXXVI, Part 4, LPI-Contrib-1234-Pt-4.

Denk, T., G. Neukum, P. Helfenstein, P. C. Thomas, E. P. Tulle, A. S. McEwen, T. Roatsch, J. Veverka, T. V. Johnson, J. E. Perry, W. M. Owen, R. J. Wagner, C. C. Porco, (2005b), The first six months of Iapetus observations by the Cassini ISS camera, 36th Lunar and Planetary Science Conference, Houston, TX, 14–18 March 2005.

Denk, T., K. D. Matz, T. Roatsch, U. Wolf, R. J. Wagner, G. Neukum, R. Jaumann, (2000), Iapetus (1): Size, topography, surface structures, craters, 31st Lunar and Planetary Science Conference, Houston, TX, March 13–17, 2000.

Dones, H. C. L., E. B. Bierhaus, K. J. Zahnle, (2009), The population of impactors on the inner Saturnian satellites, American Astronomical Society (AAS), Division for Planetary Sciences Meeting, vol. 41, abstract 41.

Elder, C., P. Helfenstein, P. Thomas, J. Veverka, J. A. Burns, T. Denk, C. Porco, (2007), Tethys' mysterious equatorial band, Bulletin of the American Astronomical Society, vol. 39, p. 429.

Filacchione, G., E. D'Aversa, F. Capaccioni, R. N. Clark, D. P. Cruikshank, M. Ciarniello, P. Cerroni, G. Bellucci, R. H. Brown, B. J. Buratti, P. D. Nicholson, R. Jaumann, T. B. McCord, C. Sotin, K. Stephan, C. M. D. Ore, (2016), Saturn's icy satellites investigated by Cassini-VIMS. IV. Daytime temperature maps, Icarus, 271, 292–313. doi: 10.1016/j.icarus.2016.02.019.

Filacchione, G., F. Capaccioni, R. N. Clark, P. D. Nicholson, D. P. Cruikshank, J. N. Cuzzi, J. I. Lunine, R. H. Brown, P. Cerroni, F. Tosi, M. Ciarniello, B. J. Buratti, M. M. Hedman, E. Flamini, (2013), The radial distribution of water ice and chromophores across Saturn's system, The Astrophysical Journal, 766, 2, 76, doi: 10.1088/0004-637X/766/2/76.

Filacchione, G., F. Capaccioni, M. Ciarniello, R. N. Clark, J. N. Cuzzi, P. D. Nicholson, D. P. Cruikshank, M. M. Hedman, B. J. Buratti, J. I. Lunine, L. A. Soderblom, F. Tosi, P. Cerroni, R. H. Brown, T. B. McCord, R. Jaumann, K. Stephan, K. H. Baines, E. Flamini, (2012), Saturn's icy satellites and rings investigated by Cassini-VIMS: III - Radial compositional variability, Icarus, 220, 2, 1064–1096, doi: 10.1016/j.icarus.2012.06.040.

Geissler, P., A. McEwen, C. Porco, D. Strobel, J. Saur, J. Ajello, R. West, (2004), Cassini observations of Io's visible aurorae, Icarus, 172, 1, 127–40, doi: 10.1016/j.icarus.2004.01.008.

Giese, B., T. Denk, G. Neukum, T. Roatsch, P. Helfenstein, P. C. Thomas, E. P. Turtle, A. McEwen, C. C. Porco, (2008), The topography of Iapetus' leading side, Icarus, vol. 193, Issue 2, pp. 359–371.

Giese, B., R. Wagner, G. Neukum, P. Helfenstein, P. C. Thomas, (2007), Tethys: Lithospheric thickness and heat flux from flexurally supported topography at Ithaca Chasma, Geophysical Research Letters, 34, 21, L21203.

Giese, B., G. Neukum, T. Roatsch, T. Denk, C. C. Porco, (2006), Topographic modeling of Phoebe using Cassini images, Planetary and Space Science, 54, 12, 1156–66, doi: 10.1016/j.pss.2006.05.027.

Glein, C. R., J. A. Baross, J. H. Waite, (2015), The pH of Enceladus' ocean, Geochimica Et Cosmochimica Acta, 162, 202–219, doi: 10.1016/j.gca.2015.04.017.

Goguen, J. D., B. J. Buratti, R. H. Brown, R. N. Clark, P. D. Nicholson, M. M. Hedman, R. R. Howell, C. Sotin, D. P. Cruikshank, K. H. Baines, K. J. Lawrence, J. R. Spencer, D. G. Blackburn, (2013), The temperature and width of an active fissure on Enceladus measured with Cassini VIMS during the 14 April 2012 South Pole flyover, Icarus, 226, 1, 1128–1137, doi: 10.1016/j.icarus.2013.07.012.

Hammond, N. P., C. B. Phillips, F. Nimmo, S. A. Kattenhorn, (2013), Flexure on Dione: Investigating subsurface structure and thermal history, Icarus, 223, 1, 418–422, doi: 10.1016/j.icarus.2012.12.021.

Hansen, C. J., A. R. Hendrix, L. W. Esposito, (2018), Observations of stellar occultations to look for plumes from Dione and Tethys, 49th Lunar and Planetary Science Conference, 19–23 March 2018, The Woodlands, TX, vol. 49, no. 2083, id 2446.

Hansen, C. J., L. W. Esposito, A. R. Hendrix, (2017), UV detection and characterization of plume activity, American Geophysical Union (AGU) Fall Meeting, abstract P23F-05.

Hansen, C. J., L. W. Esposito, B. B. Buffington, J. Colwell, A. R. Hendrix, B. K. Meinke, D. E. Shemansky, I. Stewart, R. A. West, (2011), The structure of Enceladus' plume from Cassini occultation observations, American Geophysical Union (AGU) Fall Meeting, San Francisco, CA, 5–9 December 2011.

Hansen, C. J., L. W. Esposito, A. I. F. Stewart, B. Meinke, B. Wallis, J. E. Colwell, A. R. Hendrix, K. Larsen, W. Pryor, F. Tian, (2008), Water vapour jets inside the plume of gas leaving Enceladus, Nature, 456, 7221, 477–479, doi: 10.1038/nature07542.

Hansen, C. J., L. Esposito, J. Colwell, A. Hendrix, D. Matson, C. Parkinson, W. Pryor, D. Shemansky, I. Stewart, J. Tew, Y. Yung, (2006), Enceladus' water vapour plumes, Science 311, no. 5766, pp. 1422–1425, doi: 10.1126/science.1121254.

Hansen, C. J., D. E. Shemansky, A. R. Hendrix, (2005), Cassini UVIS observations of Europa's oxygen atmosphere and torus, Icarus, 176, 2, 305–315. doi: 10.1016/j.icarus.2005.02.007.

Hansen, O. L., (1973), Ten-micron eclipse observations of Io, Europa, and Ganymede, Icarus, 18, 2, 237–246.

Harbison, R. A., P. C. Thomas, P. C. Nicholson, (2011), Rotational modeling of Hyperion, Celestial Mechanics and Dynamical Astronomy, 110, 1, 1–16. doi: 10.1007/s10569-011-9337-3.

Hedman, M. M., D. Dhingra, P. D. Nicholson, C. J. Hansen, G. Portyankina, S. Ye, Y. Dong, (2018), Spatial variations in the dust-to-gas ratio of Enceladus' plume, Icarus, 305, 123-138. doi: 10.1016/j.icarus.2018.01.006.

Hedman, M. M., C. M. Gosmeyer, P. D. Nicholson, C. Sotin, R. H. Brown, R. N. Clark, K. H. Baines, B. J. Buratti, M. R. Showalter, (2013), An observed correlation between plume activity and tidal stresses on Enceladus, Nature, 500, 7461, 182–184. doi: 10.1038/nature12371.

Helfenstein, P., P. Thomas, J. Veverka, T. Denk, G. Neukum, R. A. West, B. Knowles, C. Porco, (2005), A Cassini ISS search for regolith-texture variations on Tethys, 36th Lunar and Planetary Science Conference, Houston, TX, 14–18 March 2005.

Hemingway, D. J., M. Zannoni, P. Tortora, F. Nimmo, S. W. Asmar, (2016), Dione's internal structure inferred from Cassini gravity and topography, 47th Lunar and Planetary Science Conference, The Woodlands, TX, March 21–25, 2016, vol. 47, p. 1314.

Hendrix, A. R., G. Filacchione, C. Paranicas, P. Schenk, F. Scipioni, (2018), Icy Saturnian satellites: Disk-integrated UV-IR characteristics and links to exogenic processes, Icarus, 300, 103–114, doi: 10.1016/j.icarus.2017.08.037.

Hendrix, A. R, K. S. Noll, J. R. Spencer, (2017), Icy Saturnian satellites: Using UV-Vis data to study surface composition and surface processing, American Astronomical Society (AAS), Division for Planetary Sciences Meeting, abstract 49.

Hendrix, A. R., T. A. Cassidy, B. J. Buratti, C. Paranicas, C. J. Hansen, B. Teolis, E. Roussos, E. T. Bradley, P. Kollmann, R. E. Johnson, (2012), Mimas' far-UV albedo: Spatial variations, Icarus, 220, 2, 922–931, doi: 10.1016/j.icarus.2012.06.012.

Hendrix, A. R. and C. J. Hansen, (2010), The surface composition of Enceladus: clues from the ultraviolet, International Astronomical Union, vol. 5, Issue S263 (Icy Bodies of the Solary System) pp. 126-130, doi: 10.1017/S1743921310001626.

Hendrix, A. R. and C. J. Hansen, (2008), Ultraviolet observations of Phoebe from the Cassini UVIS, Icarus, 193, 2, 323–333.

Howett, C., J. R. Spencer, A. Verbiscer, (2017), Characterizing the heat flow from between Enceladus' tiger stripes, American Geophysical Union (AGU) Fall Meeting, abstract P43B-2881.

Howett, C. J. A., J. R. Spencer, T. Hurford, A. Verbiscer, M. Segura, (2012), Pac-Man returns: An electron-generated thermal anomaly on Tethys, Icarus, 221, 2, 1084–1088, doi: 10.1016/j.icarus.2012.10.013.

Howett, C. J., J. R. Spencer, P. Schenk, R. E. Johnson, C. Paranicas, T. A. Hurford, A. J. Verbiscer, M. Segura, (2011), A high-amplitude thermal inertia anomalies of probable magnetospheric origin in the Saturnian system, American Geophysical Union (AGU) Fall Meeting, San Francisco, CA, 5–9 Dec. 2011.

Howett, C. J. A, J. R. Spencer, J. Pearl, M. Segura, (2010), Thermal inertia and bolometric bond albedo values for Mimas, Enceladus, Tethys, Dione, Rhea and Iapetus as derived from Cassini/CIRS measurements, Icarus, 206, 2, 573–593.

Hsu, H. W., F. Postberg, Y. Sekine, T. Shibuya, S. Kempf, M. Horanyi, A. Juhasz, N. Altobelli, K. Suzuki, Y. Masaki, T. Kuwatani, S. Tachibana, S. Sirono, G. Moragas-Klostermeyer, R. Srama, (2015), Ongoing hydrothermal activities within Enceladus, Nature, 519, 7542, 207–210, plus supplemental material, doi: 10.1038/nature14262.

Iess, L., D. J. Stevenson, M. Parisi, D. Hemingway, R. A. Jacobson, J. I. Lunine, F. Nimmo, J. W. Armstrong, S. W. Asmar, M. Ducci, P. Tortora, (2014), The gravity field and interior structure of Enceladus, Science, 344, 6179, 78–80, doi: 10.1126/science.1250551.

Ingersoll, A. P. and S. P. Ewald, (2017), Decadal timescale variability of the Enceladus plumes inferred from Cassini images, Icarus, 282, 260–275, doi: 10.1016/j.icarus.2016.09.018.

Jaumann, R., K. Stephan, G. B. Hansen, R. N. Clark, B. J. Buratti, R. H. Brown, K. H. Baines, S. F. Newman, G. Bellucci, G. Filacchione, A. Coradini, D. P. Cruikshank, C. A. Griffith, C. A. Hibbitts, T. B. McCord, R. M. Nelson, P. D. Nicholson, C. Sotin, R. Wagner, (2008), Distribution of icy particles across Enceladus' surface as derived from Cassini-VIMS measurements, Icarus, 193, 2, 407–419.

Johnson, T.V. and J. I. Lunine, (2005a), Densities of the Saturnian satellites and the C/O chemistry of the solar Nebula, Bulletin of the American Astronomical Society, vol. 37, p. 704.

Johnson, T. V. and J. I. Lunine, (2005b), Saturn's moon Phoebe as a captured body from the outer solar system, Nature, 435, 7038, 69–71. doi: 10.1038/nature03384.

JPL/CalTech, Solar System Dynamics Website, Physical Data & Dynamical Constants, https://ssd.jpl.nasa.gov/?phys_data.

JPL/CalTech, Solar System Dynamics Website, Planetary Satellite Mean Orbital Parameters, https://ssd.jpl.nasa.gov/?sat_elem.

- - - - - - - - - - - - - -

Kempf, S., J. Schmidt, R. Srama, F. Postberg, F. Spahn, M. Horanyi, (2010), Enceladus dust production – new insights from Cassini, American Geophysical Union (AGU) Fall Meeting 2010, San Francisco, CA, abstract P33A-1562.

Khurana, K. K., C. T. Russell, M. K. Dougherty, (2008), Magnetic portraits of Tethys and Rhea, Icarus, 193, 2, 465–474.

Kirchoff, M. R., E. B. Bierhaus, L. Dones, S. J. Robbins, K. N. Singer, R. J. Wagner, K. J. Zahnle, (2018), Cratering Histories in the Saturnian System, Part 3: Saturn's Icy Moons, In Enceladus and the Icy Moons of Saturn, (eds.) P. M. Schenk, R. N. Clark, C. J. A. Howett, A. J. Verbiscer, J. H. Waite, The University of Arizona Press, Tucson, AZ, pp. 267–284.

Kirchoff, M. R. and P. Schenk, (2010), Impact cratering records of the mid-sized, icy saturnian satellites, Icarus, 206, 2, 485–497, doi: 10.1016/j.icarus.2009.12.007.

Kite, E. S. and A. M. Rubin, (2016), Sustained eruptions on Enceladus explained by turbulent dissipation in tiger stripes, Proceedings National Academy of Sciences, 113, 15, 3972–3975, doi: 10.1073/pnas.1520507113.

Le Gall, A. A., R. West, M. A. Jansses, C. Leyrat, L. Bonnefoy, E. Lellouch, (2017), Cassini radar and radiometry observations of Saturn's airless icy satellites, American Geophysical Union (AGU) Fall Meeting, New Orleans, LA, 11–15 December 2017, abstract P23G-02. 2017.

Lee, J. S., B. J. Buratti, M. Hicks, J. Mosher, (2010), The roughness of the dark side of Iapetus from the 2004 to 2005 flyby, Icarus, 206, 2, 623–630, doi: 10.1016/j.icarus.2009.11.008.

Levison, H. F., K. J. Walsh, A. C. Barr, L. Dones, (2011), Ridge formation and de-spinning of Iapetus via an impact-generated satellite, Icarus, 214, 2, 773–778, doi: 10.1016/j.icarus.2011.05.031.

Matson, D. L., J. C. Castillo-Rogez, A. G. Davies, T. V. Johnson, (2012), Enceladus: A hypothesis for bringing both heat and chemicals to the surface, Icarus, 221, 1, 53–62, doi: 10.1016/j.icarus.2012.05.031.

McKinnon, W. B., (2015), Effect of Enceladus's rapid synchronous spin on interpretation of Cassini gravity, Geophysical Research Letters, 42, 7, 2137–2143, doi: 10.1002/2015GL063384.

Morrison, D. and D. P. Cruikshank, (1973), Thermal properties of the Galilean satellites, Icarus, 18, 2, 224–236.

Newman, S. F., B. J. Buratti, R. H. Brown, R. Jaumann, J. Bauer, T. Momary, (2009), Water ice crystallinity and grain sizes on Dione, Icarus, 203, 2, 553–559, doi: 10.1016/j.icarus.2009.04.034.

Nimmo, F., C. Porco, C. Mitchell, (2014), Tidally modulated eruptions on Enceladus: Cassini ISS observations and models, The Astronomical Journal, 148, 3, 46, doi: 10.1088/0004-6256/148/3/46.

Ostro, S. J., R. D. West, L. C. Wye, H. A. Zebker, M. A. Janssen, B. Stiles, K. Kelleher, Y. Z. Anderson, R. A. Boehmer, P. Callahan, Y. Gim, G. A. Hamilton, W. T. K. Johnson, C. Veeramachaneni, R. D. Lorenz, Radar Team Cassini, (2010), New Cassini RADAR results for Saturn's icy satellites, Icarus, 206, 2, 498–506, doi: 10.1016/j.icarus.2009.07.041.

Ostro, S. J., R. D. West, M. A. Janssen, R. D. Lorenz, H. A. Zebker, G. J. Black, J. I. Lunine, L. C. Wye, R. M. Lopes, S. D. Wall, C. Elachi, L. Roth, S. Hensley, K. Kelleher, G. A. Hamilton, Y. Gim, Y. Z. Anderson, R. A. Boehmer, W. T. K. Johnson, (2006), Cassini RADAR observations of Enceladus, Tethys, Dione, Rhea, Iapetus, Hyperion, and Phoebe, Icarus, 183, 2, 479–90, doi: 10.1016/j.icarus.2006.02.019.

Paranicas, C., E. Roussos, R. B. Decker, R. E. Johnson, A. R. Hendrix, P. Schenk, T. A. Cassidy, J. B. Dalton III, C. J. A. Howett, P. Kollmann, W. Patterson, K. P. Hand, T. A. Nordheim, N. Krupp, D. G. Mitchell, (2014), The lens feature on the inner saturnian satellites, Icarus, 234, 155–161, doi: 10.1016/j.icarus.2014.02.026.

Paranicas, C., E. Roussos, N. Krupp, P. Kollmann, A. R. Hendrix, T. Cassidy, R. E. Johnson, P. Schenk, G. Jones, J. Carbary, D. G. Mitchell, K. Dialynas, (2012), Energetic charged particle weathering of Saturn's inner satellites, Planetary and Space Science, 61, 1, 60–65, doi: 10.1016/j.pss.2011.02.012.

Pitman, K. M., L. Kolokolova, A. J. Verbiscer, (2013), Coherent backscattering effect in Icy Satellites: Model, Cassini VIMS, and Ground-Based Near-Infrared Spectra, American Astronomical Society (AAS), Division for Planetary Sciences Meeting, abstract 45.

Porco, C., C. Mitchell, F. Nimmo, M. Tiscareno, (2018), Enceladus' plume temporal variability from analysis of Cassini ISS images, 49th Lunar and Planetary Science Conference, 19–23 March 2018, The Woodlands, TX, LPI Contribution No. 2083, id 2003.

Porco, C. C., L. Dones, C. Mitchell, (2017), Could it be snowing microbes on Enceladus? Assessing conditions in its plume and implications for future missions, Astrobiology, 17, 9, 876–901.

Porco, C., D. DiNino, F. Nimmo, (2014), How the geysers, tidal stresses, and thermal emission across the south polar terrain of Enceladus are related, The Astronomical Journal, 148, 3, 45–69, doi: 10.1088/0004-6256/148/3/45.

Porco, C. C., P. Helfenstein, P. C. Thomas, A. P. Ingersoll, J. Wisdom, R. West, G. Neukum, T. Denk, R. Wagner, T. Roatsch, S. Kieffer, E. Turtle, A. McEwen, T. V. Johnson, J. Rathbun, J. Veverka, D. Wilson, J. Perry, J. Spitale, A. Brahic, J. A. Burns, A. D. DelGenio, L. Dones, C. D. Murray, S. Squyres, (2006), Cassini observes the active south pole of Enceladus, Science, 311, 5766, 1393–1401, doi: 10.1126/science.1123013.

Porco, C. C., E. Baker, J. Barbara, K. Beurle, A. Brahic, J. A. Burns, S. Charnoz, N. Cooper, D. D. Dawson, A. D. Del Genio, T. Denk, L. Dones, U. Dyudina, M. W. Evans, B. Giese, K. Grazier, P. Helfenstein, A. P. Ingersoll, R. A. Jacobson, T. V. Johnson, A. McEwen, C. D. Murray, G. Neukum, W. M. Owen, J. Perry, T. Roatsch, J. Spitale, S. Squyres, P. C. Thomas, M. Tiscareno, E. Turtle, A. R. Vasavada, J. Veverka, R. Wagner, R. West, (2005), Cassini Imaging Science: Initial results on Phoebe and Iapetus, Science, 307, 5713, 1237–1242, doi: 10.1126/science.1107981.

Porco, C. C., R. A. West, A. McEwen, A. D. Del Genio, A. P. Ingersoll, P. Thomas, S. Squyres, L. Dones, C. D. Murray, T. V. Johnson, J. A. Burns, A. Brahic, G. Neukum, J. Veverka, J. M. Barbara, T. Denk, M. Evans, J. J. Ferrier, P. Geissler, P. Helfenstein, T. Roatsch, H. Throop, M. Tiscareno, A. R. Vasavada, (2003), Cassini imaging of Jupiter's atmosphere,

satellites, and rings, Science, vol. 299, Issue 5612, pp. 1541–1547, doi: 10.1126/science.1079462.

Postberg, F., N. Khawaja, S. Kempf, J. H. Waite, C. Glein, H. W. Hsu, R. Srama, (2017), Complex organic macromolecular compounds in ice grains from Enceladus, , 48th Lunar and Planetary Science Conference, Houston, TX, abstract 1401.

Postberg, F., J. Schmidt, J. Hillier, S. Kempf, R. Srama, (2011), A salt-water reservoir as the source of a compositionally stratified plume on Enceladus, Nature, 474, 7353, 620–622, doi: 10.1038/nature10175.

Postberg, F., S. Kempf, J. Schmidt, N. Brilliantov, A. Beinsen, B. Abel, U. Buck, R. Srama, (2009), Sodium salts in E-ring ice grains from an ocean below the surface of Enceladus, Nature, 459, 7250, 1098–1101, doi: 10.1038/nature08046.

Rathbun, J. A., J. R. Spencer, L. K. Tamppari, T. Z. Martin, L. Barnard, L. D. Travis, (2003), Galileo PPR at Io: High-resolution scans taken in conjunction with SSA and NIMS data, 34th Annual Lunar and Planetary Science Conference, March 17–21, 2003, League City, TX, abstract 385.

Royer, E. M. and A. R. Hendrix, (2014), First far-ultraviolet disk-integrated phase curve analysis of Mimas, Tethys and Dione from the Cassini-UVIS data sets, Icarus, 242, 158–171, doi: 10.1016/j.icarus.2014.07.026.

Schenk, P. M., R. N. Clark, C. J. A. Howett, A. J. Verbiscer, J. H. Waite, (2018), Enceladus and the Icy Moons of Saturn, Space Science, The University of Arizona Press in collaboration with Lunar and Planetary Institute.

Schenk, P. M., B. Buratti, P. Byrne, W. B. McKinnon, F. Nimmo, F. Scipioni, (2015), Blood stains on Tethys: evidence of recent activity, EOS p P21B-02.

Schenk, P., (2014), The colors of Enceladus: From plumes and particles to active fractures, 45th Lunar and Planetary Science Conference, The Woodlands, TX, 17–21 March 2014, LPI Contribution No. 1777, p. 2618.

Schenk, P., D. P. Hamilton, R. E. Johnson, W. B. McKinnon, C. Paranicas, J. Schmidt, M. R. Showalter, (2011), Plasma, plumes and rings: Saturn system dynamics as recorded in global color patterns on its midsize icy satellites, Icarus, 211, 1, 740–757, doi: 10.1016/j.icarus.2010.08.016.

Schmedemann, N. and G. Neukum, (2011), Impact crater size-frequency distribution (SFD) and surface ages on Mimas, 42nd Lunar and Planetary Science Conference, The Woodlands, TX, LPI Contribution No. 1608, p. 2772.

Schmidt, J., F. Postberg, N. V. Brilliantov, S. Kempf, A. Beinsen, B. Abel, U. Buck, R. Srama, (2009), On the Formation of sodium bearing E-ring ice grains on Enceladus, American Astronomical Society (AAS), Division for Planetary Sciences Meeting, abstract 41.

Scipioni, F., P. Schenk, F. Tosi, E. D'Aversa, R. Clark, J. P. Combe, C. M. D. Ore, (2017), Deciphering sub-micron ice particles on Enceladus surface, Icarus, 290, 183–200, doi: 10.1016/j.icarus.2017.02.012.

Shemansky, D. E., Y. L. Yung, X. Liu, J. Yoshii, C. J. Hansen, A. R. Hendrix, L. W. Esposito, (2014), A new understanding of the Europa atmosphere and limits on geophysical activity, The Astrophysical Journal, 797, 2, 84.

Simon, S., J. Saur, F. M. Neubauer, A. Wennmacher, M. K. Dougherty, (2011), Magnetic signatures of a tenuous atmosphere at Dione, Geophysical Research Letters, 38, 15, L15102, doi: 10.1029/2011GL048454.

Simonelli, D. P. and B. J. Buratti, (2004), Europa's opposition surge in the near-infrared: interpreting disk-integrated observations by Cassini VIMS, Icarus, 172, 1, 149–62, doi: 10.1016/j.icarus.2004.06.004.

Singer, K. N., W. B. McKinnon, P. M. Schenk, J. M. Moore, (2012), Massive ice avalanches on Iapetus mobilized by friction reduction during flash heating, Nature Geoscience, 5, 8, 574–578, doi: 10.1038/NGEO1526.

Singer, K. N. and W. B. McKinnon, (2011), Tectonics on Iapetus: Despinning, respinning, or something completely different? Icarus, 216, 1, 198–211, doi: 10.1016/j.icarus.2011.08.023.

Spencer, J. R. and T. Denk, (2010), Formation of Iapetus' extreme albedo dichotomy by exogenically triggered thermal ice migration, Science, 327, 5964, 432–435, doi: 10.1126/science.1177132.

Spencer, J. R., L. K. Tamppari, T. Z. Martin, L. D. Travis, (1999), Temperatures on Europa from Galileo photopolarimeter-radiometer: nighttime thermal anomalies, Science, 284, 5419, 1514–1516.

Spencer, J. R., (1987), The surfaces of Europa, Ganymede, and Callisto: an Investigation using Voyager IRIS thermal infrared spectra (Jupiter), The University of Arizona, Dissertation.

Spilker, L. J., (1997), Passage to a Ringed World: The Cassini-Huygens Mission to Saturn and Titan, National Aeronautics and Space Administration Technical Report, NASA-SP-533, NAS 1.21:533.

Spitale, J. N., T. A. Hurford, A. R. Rhoden, E. E. Berkson, S. S. Platts, (2015), Curtain eruptions from Enceladus' south-polar terrain, Nature, 521, 7550, 57–60, doi: 10.1038/nature14368.

Stephan, K., R. Jaumann, R. Wagner, R. N. Clark, D. P. Cruikshank, B. Giese, C. A. Hibbitts, T. Roatsch, K.-D. Matz, R. H. Brown, G. Filacchione, F. Cappacioni, F. Scholten, B. J. Buratti, G. B. Hansen, P. D. Nicholson, K. H. Baines, R. M. Nelson, D. L. Matson, (2012), The Saturnian satellite Rhea as seen by Cassini VIMS, Planetary and Space Science, 61, 1, 142–160, doi: 10.1016/j.pss.2011.07.019.

Stooke, P. J., (2002), Tethys and Dione: New geological interpretations, 33rd Annual Lunar and Planetary Science Conference, March 11–15, 2002, Houston, TX, abstract 1553.

Stooke, P. J., (1989), Tethys: Volcanic and structural geology, Lunar and Planetary Science Conference, vol. 20, p. 1071.

Tajeddine, R., N. Rambaux, V. Lainey, S. Charnoz, A. Richard, A. Rivoldini, B. Noyelles, (2014), Constraints on Mimas' interior from Cassini ISS libration measurements, Science, 346, 6207, 322–324, doi: 10.1126/science.1255299.

Tamayo, D., M. M. Hedman, J. A. Burns, (2014), First observations of the Phoebe ring in optical light, Icarus, 233, 1–8, doi: 10.1016/j.icarus.2014.01.021.

Teolis, B. D., M. E. Perry, C. J. Hansen, J. H. Waite, C. C. Porco, J. R. Spencer, C. J. A. Howett, (2017), Enceladus plume structure and time variability: Comparison of Cassini observations, Astrobiology, vol. 17, no. 9, 926–940, doi: 10.1089/ast.2017.1647.

Thomas, P. C., M. S. Tiscareno, P. Helfenstein, (2018), The Inner Small Satellites of Saturn and Hyperion, Part 3: Saturn's Icy Moons, In Enceladus and the Icy Moons of Saturn, (eds.) P. M. Schenk, R. N. Clark, C. J. A. Howett, A. J. Verbiscer, J. H. Waite, The University of Arizona Press, Tucson, AZ.

Thomas, P. C., R. Tajeddine, M. S. Tiscareno, J. A. Burns, J. Joseph, T. J. Loredo, P. Helfenstein, C. Porco, (2016), Enceladus's measured physical libration requires a global subsurface ocean, Icarus, 264, 37–47.

Thomas, P., R. Tajeddine, M. S. Tiscareno, J. A. Burns, J. Joseph, T. J. Loredo, P. Helfenstein, C. Porco, (2015), Enceladus's subsurface sea is part of a global ocean as shown by measured physical libration, American Geophysical Union (AGU) Fall Meeting, abstract P11D-05.

Thomas, P. C., J. A. Burns, M. Hedman, P. Helfenstein, S. Morrison, M. S. Tiscareno, J. Veverka, (2013), The inner small satellites of Saturn: A variety of worlds, Icarus, 226, 1, 999–1019, doi: 10.1016/j.icarus.2013.07.022.

Thomas, P. C., (2010), Sizes, shapes, and derived properties of the saturnian satellites after the Cassini nominal mission, Icarus, 208, 1, 395–401, doi: 10.1016/j.icarus.2010.01.025.

Thomas, P. C., J. A. Burns, R. Helfenstein, S. Squyres, J. Veverka, C. Porco, E. P. Turtle, A. McEwen, T. Denk, B. Giese, T. Roatsch, T. V. Johnson, R. A. Jacobson, (2007), Shapes of the saturnian icy satellites and their significance, Icarus, 190, 2, 573–584, doi: 10.1016/j.icarus.2007.03.012.

Tiscareno, M. S., J. A. Burns, J. N. Cuzzi, M. M. Hedman, (2010), Cassini imaging search rules out rings around Rhea, Geophysical Research Letters, 37, 14, L14205, doi: 10.1029/2010GL043663.

Tokar, R. L., R. E. Johnson, M. F. Thomsen, E. C. Sittler, A. J. Coates, R. J. Wilson, F. J. Crary, D. T. Young, G. H. Jones, (2012), Detection of exospheric O2+ at Saturn's moon Dione, Geophysical Research Letters, 39, 3, L03105, doi: 10.1029/2011GL050452.

Tortora, P., M. Zannoni, D. Hemingway, F. Nimmo, R. A. Jacobson, L. Iess, M. Parisi, (2016), Rhea gravity field and interior modeling from Cassini data analysis, Icarus, 264, 264–273, doi: 10.1016/j.icarus.2015.09.022.

Verbiscer, A. J., Helfenstein, P., Buratti, B. J., and Royer, E., (2018), Surface Properties of Saturn's Icy Moons from Optical Remote Sensing, Part 3: Saturn's Icy Moons, In Enceladus and the Icy Moons of Saturn, (eds.) Schenk, P. M., Clark, R. N., Howett, C. J. A., Verbiscer, A. J., and Waite, J. H., The University of Arizona Press, Tucson, AZ.

Wagner, R. J., G. Neukum, U. Wolf, N. Schmedemann, T. Denk, K. Stephan, T. Roatsch, C. C. Porco, (2011), Bright ray craters on Rhea and Dione, 42nd Lunar and Planetary Science Conference, March 7–11, 2011, Houston, TX, LPI Contribution no. 1608, p.2249.

Wagner, R. J., G. Neukum, B. Giese, T. Roatsch, T. Denk, U. Wolf, C. C. Porco, (2010), The geology of Rhea; a first look at the ISS camera data from orbit 121 (Nov. 21, 2009) in Cassini's extended mission, 41st Lunar and Planetary Science Conference XLI, March 1–5, 2010, The Woodlands, TX, LPI Contribution no. 1533, p.1672.

Wagner, R. J., G. Neukum, B. Giese, T. Roatsch, T. Denk, (2007), Geology and Geomorphology of Rhea: a First Look at the High-Resolution Cassini ISS Images from the Targeted Flyby on Aug. 30, 2007, American Geophysical Union (AGU) Fall Meeting, abstract P12B-06.

Waite, J. H., C. R. Glein, R. S. Perryman, B. D. Teolis, B. A. Magee, G. Miller, J. Grimes, M. E. Perry, K. E. Miller, A. Bouquet, J. I. Lunine, T. Brockwell, S. J. Bolton, (2017), Cassini finds molecular hydrogen in the Enceladus plume: Evidence for hydrothermal processes, Science, 356, 6334, 155–159, doi: 10.1126/science.aai8703.

Yeoh, S. K., Z. Li, D. B. Goldstein, P. L. Varghese, D. A. Levin, L. M. Trafton, (2017), Constraining the Enceladus plume using numerical simulation and Cassini data, Icarus, 281, 357–378, doi: 10.1016/j.icarus.2016.08.028.

Zhang, Z., A. G. Hayes, M. A. Janssen, P. D. Nicholson, J. N. Cuzzi, I. de Pater, D. E. Dunn, (2017), Exposure age of Saturn's A and B rings, and the Cassini Division as suggested by their non-icy material content, Icarus, 294, 14–42, doi: 10.1016/j.icarus.2017.04.008.